High Resolution MIMO Radar Sensing With Compressive Illuminations

Nithin Sugavanam , Siddharth Baskar, and Emre Ertin

Abstract—We present a compressive radar design that combines multitone linear frequency modulated (LFM) waveforms in the transmitter with a classical stretch processor and sub-Nyquist sampling in the receiver. The proposed compressive illumination scheme has fewer random elements resulting in reduced storage and complexity for implementation and calibration than previously proposed compressive radar designs based on stochastic waveforms. We analyze this illumination scheme for the task of a joint range-angle of arrival estimation in the multi-input and multi-output (MIMO) radar system. We present recovery guarantees for the proposed illumination technique. We show that for a sufficiently large number of modulating tones, the system achieves high-resolution in range and successfully recovers the range and angle-of-arrival of targets in a sparse scene. Furthermore, we demonstrate the stability of recovery of targets in range and angle of arrival domain in the continuum. Finally, we present simulation results to illustrate the recovery performance as a function of system parameters.

Index Terms—Compressive sensing, mutual coherence, restricted isometry property, structured measurement matrix, linear frequency modulated waveform, radar.

I. INTRODUCTION

ADAR imaging systems acquire information about the scene of interest by transmitting pulsed waveforms and analyzing the received backscatter energy to estimate the range, angle of arrival, Doppler velocity, and scattering coefficient of the reflectors in the scene. These range profiles from multiple pulses and multiple antenna elements can be processed jointly to solve many inference tasks, including detection, tracking, and classification [1]–[4]. We analyze a coherent MIMO radar system with closely separated antennas. The angle of arrival of each scattering center in the scene is approximately the same for all phase-centers. The main advantage of coherent MIMO radar is its ability to synthesize a sizable virtual array with fewer antenna elements for improved spatial processing. Additionally, MIMO radar systems with multiple transmit and receive elements employing independent waveforms on transmitter provide

Manuscript received July 28, 2021; revised December 29, 2021 and February 21, 2022; accepted February 23, 2022. Date of publication March 7, 2022; date of current version March 25, 2022. The associate editor coordinating the review of this manuscript and approving it for publication was Prof. Pascal Vallet. This work was supported in part by Army Research Office Grant W911NF-11-1-0391 and NSF Grants IIS-1231577, CNC-823070, and CBET-2037398. (Corresponding author: Nihin Sugavanam.)

The authors are with the Electrical and Computer Engineering Department, The Ohio State University, Columbus, OH 43210 USA (e-mail: sugavanam.3@osu.edu; baskar.3@osu.edu; ertin.1@osu.edu).

This article has supplementary downloadable material available at https://doi.org/10.1109/TSP.2022.3156731, provided by the authors.

Digital Object Identifier 10.1109/TSP.2022.3156731

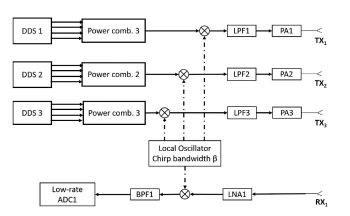


Fig. 1. Effect of stretch processing, which transforms the task of delay estimation to a task of spectral estimation.

spatial processing gains by exploiting the diversity of channels between the target and radar [5], [6]. This work estimates the range, angle of arrival, and scattering-coefficient of reflectors in the scene using a MIMO radar system with N_T transmitters and N_R receivers. The i^{th} transmitter utilizes a modulated wideband pulse $s_i(t)$ of bandwidth B and pulse duration τ . By assuming that the support of the observed delays are known to lie on an interval T_u (termed as range swath in radar literature), the received signal at receiver r can be expressed as

$$y_r(t) = \sum_{k=1}^K \sum_{i=1}^{N_T} \alpha_R(\bar{\theta}_k, r) \alpha_T(\bar{\theta}_k, i) s_i(t - \bar{\Delta}_k) \bar{x}_k + w_l(t),$$

where $w_l(t)$ is the additive receiver noise, $\bar{\Delta}_k$ is the round-trip delay time, x_k is the complex scattering coefficient of k^{th} target, and $\alpha_R(\bar{\theta}_k, r)$ and $\alpha_T(\bar{\theta}_k, i)$ is the array factor for the r^{th} receiver and the i^{th} transmitter, which is a function of the angle of arrival $\bar{\theta}_k$. Conventionally, matched filtering is performed to estimate the unknown parameters associated with the targets in the scene. However, the matched filter's implementation requires Nyquist rate sampling, which is proportional to the bandwidth of the transmitted signal. This sampling rate severely limits the resolution and dynamic range of the Analog to Digital Converter (ADC) needed for direct digital implementation of the radar since the resolution of the ADC is inversely proportional to the maximum sampling rate [7]. Stretch processing is an approximation of the matched filter that can be implemented in the analog domain for the case of linear frequency modulated waveform (LFM) denoted by $s(t) = \exp(jBt^2/\tau)$. This approximation of matched filter is implemented by mixing the received signal with a reference LFM waveform using an analog mixer, and subsequently, low-pass filtering the mixer output. At the receiver output, the waveform delayed by Δ appears as a sinusoidal tone whose frequency is given by $B\Delta$ as shown in Fig. 1. Stretch processing [1], [8] can result in a substantial reduction in sampling rate for the ADC used in the receiver if the delay support T_u is smaller than the pulse length τ . Furthermore, the

1053-587X © 2022 IEEE. Personal use is permitted, but republication/redistribution requires IEEE permission. See https://www.ieee.org/publications/rights/index.html for more information.

received signal at the stretch processor's output can be written as $y(t) = \sum_{k=1}^K \bar{x}_k \exp(jB\bar{\Delta}_k t/\tau) + w(t)$.

A. Prior Work

Compressive sensing's (CS) success in solving inverse problems relies on establishing recovery guarantees on the measurement operator and developing tractable and efficient recovery algorithms. The two forms of recovery guarantees in the literature are known as uniform and non-uniform recovery guarantees. Uniform guarantees imply the successful recovery of all K-sparse vectors for any realization of the system parameters chosen at random. Such guarantees rely on the restrictive isometry property (RIP). If the sensing operator satisfies the RIP property of order 2K, given by $\delta_{2K} \leq \delta \approx \sqrt{2} - 1$ with high probability then all K-sparse vectors are successfully recovered, with a reconstruction error of an oracle estimator that knows the support of the sparse vector or the support of K largest elements [9], [10] up to a logarithmic factor of the size of the search space. Non-uniform guarantees imply that almost all system realizations recover a fixed K-sparse vector successfully. These guarantees impose conditions on the spectral norm, and mutual coherence of the measurement operator for successful recovery of a K-sparse vector [11]. Furthermore, there are numerous tractable algorithms, with provable performance guarantees, that is based on convex relaxation on the discretized space [12], [13], or the continuous parameter space in [14], [15], or greedy methods [16], [17] and data-driven methods that utilize unrolled networks [18]–[20] to solve the linear inverse problem. Motivated by these advances, compressed sensing techniques have been applied to a variety of problems in radar signal processing [21]-[23]. Next, we discuss existing architectures in the literature that solve the radar imaging problem.

Xampling Based radar: The problem of range profile estimation [24] is solved using filter-banks to acquire low-rate sub-Nyquist samples. A parallel research thrust [25] provided an average case recovery guarantee for the problem of the angle of arrival estimation with randomly located antenna elements, under the idealized assumption of orthogonality between received waveform from different range bins. Furthermore, frequency division multiple access based waveforms with sub-Nyquist sampling strategies in fast and slow-time are employed in [26]-[29] for estimating the range, angle of arrival and velocity. The Xampling framework [27], [30] has also been implemented as a practical system in [31]. These systems require multiple channels per receiver that perform filtering and analog compression and with individual ADCs for each channel to acquire the resultant Fourier coefficients. Alternatively, a single ADC per receiver channel with foldable multi-band sampler ADC utilizing carefully chosen frequency bands at transmitter to recover the Fourier coefficients from sub-Nyquist sampling has been also analyzed. This approach leads to a drastic increase in the complexity of receiver design with a system employing multiple transmitters and receivers.

Stepped frequency radar: The problem of waveform design using frequency hopping codes for estimation in range, velocity, and angle domain is solved in [32] using mutual coherence as the objective. A similar guarantee for successful estimation of range, angle of arrival, and velocity using stepped frequency

multi-pulse MIMO radar in each transmitter has been presented in [33], [34]. The problem of sub-sampling in array elements is also posed as a matrix completion problem in the grid-less estimation setting in [35], [36] and a condition is established on the number of antenna elements that need to be observed to recover the entire low-rank data matrix. Random frequencyagile radar [37], [38] utilizes a random sequence of frequency steps over a coherent processing interval (CPI) to estimate the range and velocity of targets. The work in [37] formulates the problem of designing the frequency codes such that the lower bound on the Mean square error is minimized. The recovery guarantees for successful recovery from M possible frequency steps transmitted over N pulses is established as $\mathcal{O}(\sqrt{\frac{M}{\log(MN)}})$ targets is presented in [38]. This guarantee is further refined [39] to guarantee successful recovery of $\mathcal{O}(\frac{M}{N\log(MN)})$ targets. Frequency agile radar framework has been utilized in a phasedarray radar [40]. The system employs transmit and receive beam-forming to solve the range, angle of arrival, and velocity estimation. Sparse stepped frequency radar with Doppler division multiplexing for range, velocity, azimuth, and elevation estimation using sparse 2D arrays [41] has been proposed for automotive radar applications. A reduced coherent processing interval is considered in [42] without any deterioration in the recovery guarantee. Step-frequency-radar systems have a short unambiguous range $R_u = \frac{c}{2\Delta F}$ governed by the frequency step size ΔF , a condition exacerbated by sparse sampling schemes. In addition, range gating is impractical for many domains as it needs to be implemented using ultra-fast switches in the time domain. As a result, step frequency radars are reserved for shortrange applications such as level gauging, ground-penetrating radar, and instrumentation. Finally, the standard single local oscillator implementation requires the pulse (frequency step) repetition interval to be larger than the round-trip time between the radar platform and the scene center. As a result, long-range radar systems for search, detection, and tracking do not utilize step-frequency designs.

Stochastic waveform based radar: The conditions for successful recovery of target parameters for single pulse systems utilizing stochastic waveforms are established in [43]. These results are extended to single pulse multiple transmit and receive system for range, Doppler-velocity and azimuth estimation and target detection in [44]-[47]. A common approach based on stochastic waveforms [48] in the time domain and [49] in the frequency domain have been implemented and analyzed. Baraniuk et al. in [50] have shown that random matrices with i.i.d entries from either Gaussian or sub-Gaussian probability distribution satisfy the RIP condition, such that for any $\delta \in [0,1]$ $\delta_K \leq \delta$ if number of measurements $M \sim \mathcal{O}(K \log(N/K))$. Although these unstructured random matrices have remarkable recovery guarantees, they do not represent any practical measurement scheme, which leads us to consider classical linear time-invariant (LTI) systems. This constraint leads to a structured matrix of either a partial or sub-sampled Toeplitz or circulant matrix. The RIP condition of order K for partial Toeplitz matrices in the context of channel estimation was established by Haupt et al. in [51]. They showed that if the number of measurements $M \sim \mathcal{O}(K^2 \log N)$, then $\delta_K \leq \delta$. This quadratic scaling of measurements with respect to sparsity was improved in [49], [52], [53]. Romberg in [49] considered an active imaging system that used waveform with a random symmetric frequency spectrum and acquired compressed measurements using random subsampler or random demodulator at the receiver to estimate the sparse scene. The resultant system is a randomly sub-sampled circulant matrix representing the convolution and compression process. It is shown that for a given sparsity level K, the condition that $\delta_{2K} \leq \delta$ is satisfied if the number of measurements $M \ge \alpha_6 \delta^{-2} \min(K(\log N)^6, (K \log N)^2)$, where $\alpha_6 >$ 0 is a universal constant independent of the size of problem and δ . This result was extended by *Rauhut* et al. in [52]. They consider a deterministically sampled random waveform in the time domain with samples following Rademacher distribution, which is modeled as a sub-sampled Toeplitz or Circulant matrix with entries sampled from Rademacher distribution. It was shown that for a given sparsity level K, $\delta_K \leq \delta$ with high probability if the number of measurements $M \ge$ $\alpha_7 \max(\delta^{-1}(K \log N)^{3/2}, \delta^{-2}K(\log N \log K)^2)$, where α_7 is a universal constant. In the subsequent work by Krahmer et al. in [53], the relation between sparsity level and the number of measurements is improved, and more general random variables are considered, such as vectors following sub-Gaussian distribution to generate the Toeplitz or Circulant matrix. It is shown that, for a given sparsity level K the condition $\delta_K \leq \delta$ is satisfied if the number of measurements $M \ge \alpha_8 \delta^{-2} K (\log K \log N)^2$, where the constant α_8 is a function of only the sub-Gaussian norm of the random variables generating the matrix. The measurement operator generated from these systems guarantees successful recovery at the expense of increased design complexities. The memory requirements for generating and storing these waveforms are largely due to the high bandwidth requirements. In addition, the peak to average power ratio (PAPR) of these waveforms is large, leading to non-linearity in the operation of the power amplifiers required in practical systems.

Random demodulator based radar: The random demodulator (RD) involves modulation of the received wide-band signal with pseudo-random sequences followed by a low-pass filter or an integrator to obtain low-rate sub-Nyquist samples. Such systems also guarantee the successful recovery of multi-tone spectra with high probability. This waveform system [54] has also been implemented in practice in [55]. Generating and mixing with pseudo-random sequences at high rates is a challenging task and leads to signal-dependent uncertainties due to timing imperfections as studied in [56], [57].

B. Contributions

There is a vast body of literature on sparse recovery algorithms for radar detection and estimation problems. In contrast, much less attention has been devoted to the *design* frameworks for compressive sensing systems for Radar with provable performance, with the notable exception of the seminal Xampling framework discussed in prior work. However, the performance of the algorithmic work is critically dependent on the availability of sub-Nyquist samples from a well-conditioned sensing operator realizable in hardware. This work aims to fill this gap by introducing an alternative novel compressive radar sensing framework with many implementation advantages making it suitable for long-range, high power radar systems deployed for

TABLE I INDEX OF NOTATIONS AND TERMS

Symbol	Description			
β	Bandwidth of the Chirp Signal (Hz)			
$\mid B \mid$	Bandwidth available for transmission (Hz)			
T_u	Unambiguous round-trip time (s)			
τ	pulse duration of transmitted signal (s)			
F_s	Sampling rate at the receiver, $F_s = \beta \frac{\tau}{T_u}$ (Hz)			
K	Number of dominant scattering centers			
k	index of scattering centers, $k = 1, \dots, K$			
$\begin{vmatrix} k \\ \bar{\theta}_k \end{vmatrix}$	angle of arrival of arrival of scattering center $k \ \overline{\theta}_k \in [0, 2\pi]$			
$ \bar{\Delta}_k $	round-trip time of scattering center $k \ \bar{\Delta}_k \in [0, T_u]$			
N_T	Number of transmitters			
N_R	Number of receivers			
N_c	Number of modulating tones used per transmitter			
i	index of the transmitter $i = 1, \dots, N_T$			
r	index of the receiver $r = 1, \cdots, N_R$			
n_c	index for the modulating tone $n_c = 1, \dots, N$			
$\mid n \mid$	index for the range bin			
v	index for the angle of arrival bin			
N	Number of bins in the range-domain $N = BT_u$			
N_{θ}	Number of bins in the angle of arrival domain			
M	Number of samples per in time domain $M = \beta T_u$			
$\mid m \mid$	index of the samples $m = 0, \dots, M-1$			
y _r	Samples at receiver $r, \mathbf{y_r} \in \mathbb{C}^M$			
$s_i(t)$	Transmitted signal at transmitter i			
c	velocity of light in free-space			
f_c	Center Carrier frequency			
λ_c	Wavelength at center frequency $\lambda = \frac{f_c}{c}$			
f	$\mathbf{f} = [f_1, \dots, f_N]$ is the set of modulating frequencies where			
	$f_n = \frac{nB}{N} \in [0, B]$			
d_T	spacing between transmitter antenna elements			
d_R	spacing between receiver antenna elements			
$\alpha_T(\theta, i)$	Transmitter steering vector for element i at the angle θ			
$\alpha_R(\theta,r)$	Receiver steering vector for element \boldsymbol{r} at the angle $\boldsymbol{\theta}$			

search, detection, and tracking. The proposed waveforms derived from the LFM waveform is derived from a chirp waveform that sweeps a bandwidth of $\beta < B$. This compressive radar structure termed compressive illumination was first proposed in [62]. This work utilized a linear combination of sinusoids to modulate an LFM waveform with randomly selected center frequencies at the transmitter while maintaining the simple standard stretch processing receiver structure. We observe that under the proposed compressive sensor design, each delayed copy of the transmitted waveform is mapped to a multi-tone spectra with a known structure. We show that this known multitone frequency structure enables recovery of range profile from aliased time samples with provable guarantees complementing previous work with a single transmitter and receiver [63], [64] which has shown good empirical performance using simulations and practical implementation in [65]. In our earlier work, we established that $\mathcal{O}(K^2 \log(N))$ measurements recover the range and scattering coefficient of K dominant scattering centers. Additionally, the number of modulating tones needs to scale in proportion to the size of the search space. In this work, we extend this approach to a MIMO setup. We establish that by scaling the number of transmitters N_T , the number of modulating tones scale as $\mathcal{O}(\frac{N}{N_T})$, and enable the estimation of range and angle of arrival.

• Theoretical uniform and non-uniform guarantees: The system proposed in this work achieves near-optimal scaling in the number of measurements up to an additional logarithmic factor for non-uniform guarantees as shown in Table III. We also established that for the sensing scheme to satisfy RIP of order K, we need $\mathcal{O}(K\delta^{-2}\log(N/K))$ measurements.

Matrix Type of size $M \times N$ Mutual CoherenceSpectral NormReferenceRandom matrix (NM) independent random entries $2\sqrt{\frac{\log N}{M}}$ (ideal operator) $\sqrt{\frac{N}{M}} + 1$ [58], [11], [59]Toeplitz block matrix with (N+M) random entries $\mathcal{O}\left(\sqrt{\frac{\log N}{M}}\right)$ $\mathcal{O}\left(\sqrt{\frac{N}{M}}\right)$ [60]Frequency agile radar $\mathcal{O}\left(\sqrt{\frac{\log N}{M}}\right)$ -[38], [42]LFM waveform modulated with $N_c \ll N$ randomly selected tones $\mathcal{O}\left(\sqrt{\frac{\log N}{M}}\right)$ $\mathcal{O}\left(\sqrt{\frac{N}{M}}\log(N)\right)$ This work

TABLE II
MEASURES THAT CHARACTERIZE SENSING MATRICES

 ${\bf TABLE~III}\\ {\bf SUPPORT~RECOVERY~GUARANTEES~FOR~DIFFERENT~SENSING~MATRICES}$

Recovery Guarantees from noisy measurements with component-wise noise variance		1 MC -111	D . C
-	Sparsity condition	Minimum signal	Reference
Random matrix with (NM) independent random entries (ideal operator)	$O\left(\frac{M}{\log N}\right)$	$\mathcal{O}\left(\sigma\sqrt{2\log N}\right)$	[11]
Toeplitz block matrix with $(N+M)$ random entries	$O\left(\frac{M}{\log N}\right)$	$\mathcal{O}\left(\sigma\sqrt{2\log N}\right)$	[60]
Xampling based radar	$\mathcal{O}(\sqrt{M})$	-	[61], [27], [26]
Frequency agile radar	$O(\sqrt{\frac{M}{\log(MM)}})$	-	[38]
LFM waveform modulated with $N_c \ll N$ randomly selected tones		$\mathcal{O}\left(\sigma\sqrt{2\log N}\right)$	This work

- Ease of calibration: The key advantage of the proposed radar system is $2N_c$ parameters that denote the phase and frequencies of the modulating waveforms that need to be stored. The transmitter has low memory requirements for waveform generation because the modulating tones are generated using a direct digital synthesizer. Typically the mismatches in waveforms with a significant number of parameters complicate the calibration process. In our case, the phase mismatches in the transmit and receive channels lead to false-positive detections. We formulated and solved the phase calibration problem in [66] to jointly calibrate the phase mismatches and estimate the range and angle of arrival of targets. Furthermore, a transmitter using a single Linear frequency-modulated waveform sweeping a bandwidth B to improve the range-resolution is impaired by non-linearity in the sweep [67], [68]. These non-linearities cause degradation in range-resolution [69]. These nonlinearities are typically corrected by using pre-distortion techniques. On the contrary, the proposed system sweeps a smaller bandwidth β , which minimizes the effects of non-linearity in a sweep on system performance.
- Reduced complexity of receiver with low-sampling rate ADC: The stretch-processor is an analog approximation of the matched filtering. Even though the stretch processor uses a single LFM waveform with bandwidth B, unambiguous delay swath T_u and pulse duration τ lead to a reduction in sampling rate given by $F_s = \frac{BT_u}{\tau}$. In case of long-range surveillance and imaging [70], $\frac{T_u}{\tau} = 0.3$, therefore the sampling rate is $F_s = 0.3B$, which is significantly large. We utilize uniform sampling ADCs operating at a low sampling rate $F_s = \beta \frac{T_u}{\tau}$ since that is the bandwidth of the possible beat frequencies due to a single modulated waveform. This bandwidth β can be chosen to scale with the scene's complexity, thereby reducing the sampling rate of the system.

Table II summarizes the characteristics of some well-studied random sensing schemes as well as our proposed scheme. Table III summarizes the support recovery guarantees for these random sensing schemes as well as our proposed scheme. The rest of the paper is organized as follows, Section II states the signal model, Section III states the main recovery guarantee, Section V provides simulation verification of our theoretical results.

II. SYSTEM MODEL

A. System Setup

We consider N_T transmitters and N_R collocated receivers that function as a MIMO radar system. This system employs the compressive illumination framework proposed in [62], [64], and [71], which is extended to the case of multiple transmitters and receivers for estimating the target range and angle of arrival. The transmitter antenna elements are placed with a spacing of $d_T = 0.5$ and the receiver antenna elements are placed with a spacing of $d_R = 0.5N_T$ relative to the wavelength $\lambda_c = c/f_c$ of the carrier signal. We obtain the virtual array with an aperture length $(N_T N_R - 1)\lambda_c/2$ meter, where c is the velocity of light in vacuum, and f_c is the carrier frequency. The process used to generate the transmitted signal is shown in Fig. 3. We discretize the frequency range [0, B] into N frequencies f_1, \ldots, f_N , where $N=Bt_u$, t_u is the unambiguous time interval, B is the system bandwidth, and $f_{n_c}=f_c+\frac{n_cB}{N}$. A subset of N_cN_T tones are chosen at random from these N possible frequencies, where N_c is the number of modulating tones used in each transmitter. The chosen tones are used for modulating the LFM waveform with bandwidth $\beta \ll B$, using the Single Side-Band (SSB) modulation technique as shown in Fig. 3. We simplify this selection model for analysis by considering N independent indicator random variables $\hat{\gamma}_{n_c} \in \{0,1\}$ following a Bernoulli distribution with

$$\hat{\gamma}_{n_c} = \left\{ \begin{array}{c} 1 \text{ with probability } N_c N_T/N \\ 0 \text{ with probability } 1 - N_c N_T/N \end{array} \right.$$

to select the tones that modulate the LFM waveform such that N_cN_T waveforms are selected on an average. Each chosen LFM waveform is scaled by an independent and

identically distributed complex exponential with a uniformly distributed phase such that the probability density function $f_{\Phi}(\phi_{n_c})=1/(2\pi), \phi_{n_c}\in[0,2\pi].$ We define the sequence of random variables $\{\hat{c}_1,\ldots,\hat{c}_N\}$ that model this selection process where

$$\hat{c}_{n_c} = \hat{\gamma}_{n_c} \exp(j\Phi_{n_c}). \tag{1}$$

Each selected waveform is assigned to one of the N_T transmitters using a deterministic rule. The transmitted signal from the transmitter i can be written as

$$s_i(t) = \sum_{n_c=1}^{N} \hat{c}_{n_c} \frac{\exp\left(j2\pi \left[f_{n_c}t + \frac{\beta}{2\tau}t^2\right]\right)}{\sqrt{N_c N_T}} rect\left(\frac{t - \frac{\tau}{2}}{\tau}\right),$$

where $rect((t-\frac{\tau}{2})/\tau)=1$ if $t\in(0,\tau)$ and 0 otherwise. The received signal at receiver r due to a scattering center located at a round-trip delay of $\Delta\in[0,t_u]$ and angle of arrival $\bar{\theta}\in[0,2\pi]$ is given by

$$rx_r(t) = \sum_{n_c=1}^{N} \hat{c}_{n_c} x \frac{\exp\left(j2\pi \left[f_{n_c}(t-\Delta) + \frac{\beta}{2\tau}(t-\Delta)^2\right]\right)}{\sqrt{N_c N_T}}$$

$$\exp\left(j2\pi\frac{f_c}{c}\sin(\bar{\theta})\left(\lambda_c d_T \xi(n_c) + \lambda_c d_R r\right)\right) rect\left(\frac{t - \frac{\tau}{2}}{\tau}\right),$$

where $\xi(n_c)$ is the index of the transmitter assigned to the carrier f_{n_c} . The angle of arrival is denoted by $\theta = \sin(\bar{\theta}) \in [-1,1]$. After stretch processing the signal is given by

$$y_r(t) = \sum_{n=1}^{N} \hat{c}_{n_c} x \frac{\exp\left(j2\pi \left[-f_{n_c} \Delta + \left(f_{n_c} - \frac{\beta}{\tau} \Delta\right) t\right]\right)}{\sqrt{N_c N_T}}$$

$$\exp\left(j2\pi\theta\left(d_T\xi(n_c) + d_Rr\right)\right)rect\left(\frac{t - \frac{\tau}{2}}{\tau}\right). \tag{2}$$

Fig. 4 shows the stretch processing operation implemented at a particular receiver. The sampling rate at the receiver after stretch processing is $F_s = \beta t_u/\tau$, which leads to $M = \beta t_u$ samples at stretch processor output at each receiver. Since the sampling rate is much lower than the Nyquist rate required for the modulating tones, the multi-tone frequency spectrum corresponding to a target with a delay of Δ aliases to the range $[-F_s/2, F_s/2]$. In the following sections, we show that the delay and angle of arrival of a sparse set of targets can be uniquely recovered if a sufficient number of modulating tones are utilized in the transmitter. The m^{th} sample $y_r(m)$ at the stretch processor at receiver r due to a target with round-trip delay of $\Delta \in [0, t_u]$ and an angle of arrival $\theta \in [0, 2\pi]$ with amplitude $x \in \mathbb{C}$ is given by

$$\begin{split} y_r(m) &= \sum_{n_c=1}^N \hat{c}_{n_c} \exp\left(-j2\pi f_{n_c}\Delta\right) \alpha_R(\theta; r) \frac{\alpha_T(\theta; \xi(n_c)) x}{\sqrt{N_T N_R N_c M}} \\ &\exp\left(j2\pi \left(f_{n_c} - \frac{\beta \Delta}{\tau}\right) \frac{m}{F_s}\right) + w_{r,m}, \\ \alpha_T(\theta; \xi(n_c)) &= \exp\left(j2\pi d_T \xi(n_c)\theta\right), \\ \alpha_R(\theta; r) &= \exp\left(j2\pi d_R r\theta\right), \end{split}$$

where $w_{r,m}$ is the m^{th} noise sample at receiver r, $\alpha_R(\theta; r)$ is the array steering parameter corresponding to receiver r,

and $\alpha_T(\theta; \xi(n_c))$ is the steering parameter corresponding to the chosen transmitter specified by the rule $\xi(n_c)$ for the n_c^{th} waveform. We present the recovery guarantees for the proposed system by discretizing the range-angle of arrival space. We also present an algorithm that recovers the range and angle of arrival of a sparse set of targets in the continuum in section IV. The unambiguous interval from $[0,t_u]$ is discretized at a resolution of 1/B corresponding to the resolution achieved by a system employing a signal of bandwidth B resulting in $N=Bt_u$ bins. Each delay bin is denoted as $\Delta_n=n/B, n=0,1,\ldots,N-1$. The angle of arrival characterized by $\cos\theta\in[-1,1]$ is partitioned into $N_\theta=N_TN_B$ grids. Each angle bin is denoted as

$$\theta_v \in \{2v/(N_T N_R) | v = -N_T N_R/2, \dots, N_T N_R/2 - 1\}.$$

The receiver and transmitter steering vectors as function of the angle of arrival θ_v are defined as

$$\alpha_{\mathbf{R}}(\theta_v) = \begin{bmatrix} 1 & \cdots & \exp\left(j\bar{d}_R(N_R - 1)\theta_v\right) \end{bmatrix}^T$$
, and $\alpha_{\mathbf{T}}(\theta_v) = \begin{bmatrix} 1 & \cdots & \exp\left(j\bar{d}_T(N_T - 1)\theta_v\right) \end{bmatrix}^T$,

respectively, where $\bar{d}_R = 2\pi d_R$, and $\bar{d}_T = 2\pi d_T$. The normalized sample at the stretch processor output $y_r(m)$ at receiver r due to the targets in the region of interest is given by

$$y_r(m) = \sum_{\substack{v=1\\n=0}}^{v=N_T N_R} \sum_{n_c=1}^{n_c=N} \hat{c}_{n_c} \alpha_R(\theta_v; r) \frac{\alpha_T(\theta_v; \xi(n_c)) x(v, n)}{\sqrt{N_T N_R N_c M}}$$

$$\exp\left(-j2\pi f_{n_c}\Delta_n\right)\exp\left(\frac{j2\pi m}{F_s}\left(f_{n_c}-\frac{\beta\Delta_n}{\tau}\right)\right)+w_{r,m},$$

where $r=1,\ldots,N_R, m=0,\cdots M-1$, and $x_{v,n}\in\mathbb{C}$ is the scattering coefficient at range bin n and angle of arrival bin v. The concatenated output from all the N_R receivers can be compactly written as

$$y = Ax + w, (3)$$

where the signal is given by

$$\mathbf{y} = [\mathbf{y}_1 \cdots \mathbf{y}_{N_R}]^T, \mathbf{y}_r = [y_r(0) \cdots y_r(M-1)]^T \in \mathbb{C}^M.$$

$$\mathbf{w} = [\mathbf{w}_1 \cdots \mathbf{w}_{N_R}]^T, \mathbf{w}_r = [w_{r,0} \cdots w_{r,M-1}]^T \in \mathbb{C}^M.$$

is the zero mean additive white Complex Gaussian noise with variance σ^2 , and $\mathbf{x} \in \mathbb{C}^{NN_TN_R}$ contains the complex scattering amplitudes associated with targets at all possible grid locations in the range-angle domain. The sensing matrix $\mathbf{A} \in \mathbb{C}^{N_RM \times N_\theta N}$ can be expressed as a series of deterministic matrices with random coefficients as follows

$$\mathcal{A} = \sum_{n_c=1}^{N} \hat{c}_{n_c} \left(\bar{\alpha}_{\mathbf{R}} \bar{\alpha}_{\mathbf{T}}(\xi(\mathbf{n_c})) \right) \otimes \left(\mathbf{H}_{n_c} \bar{\mathbf{A}} \mathbf{D}_{n_c} \right),$$
where, $\bar{\alpha}_{\mathbf{R}} = \sqrt{1/(N_R N_T)} \left[\alpha_{\mathbf{R}}(\theta_1) \quad \cdots \quad \alpha_{\mathbf{R}}(\theta_{N_{\theta}}) \right]$

$$\bar{\alpha}_{\mathbf{T}}(\xi(\mathbf{n_c})) = \operatorname{diag} \left(\exp \left(j \bar{d}_T \xi(n_c) \theta_1 \cdots \exp \left(j \bar{d}_T \xi(n_c) \theta_{N_{\theta}} \right) \right) \right) \tag{4}$$

for $n_c = 0, ..., N - 1$. $\bar{\alpha}_{\mathbf{R}} \in \mathbb{C}^{\mathbf{N}_{\mathbf{R}} \times \mathbf{N}_{\theta}}$ is the matrix consisting of receiver steering vectors for all the bins of angle of arrival,

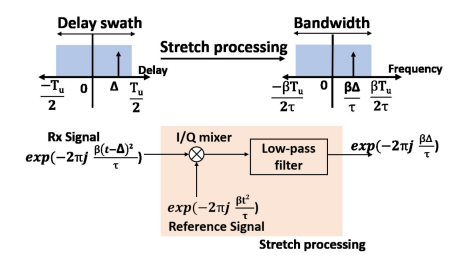


Fig. 2. Block diagram of the transmitter and receiver. The Direct digital synthesizer (DDS) generates modulating sinusoidal tones used for modulating the LFM signal. The power combiner (Power Comb) is used to generate the multi-tone signal and modulated with the LFM signal using a single-sideband modulation technique using the low-pass filter (LPF). The receiver consists of a low noise amplifier and it is mixed with the reference LFM signal to obtain the multi-tone signal and filtered using the band-pass filter (BPF) to sample using a low-rate ADC.

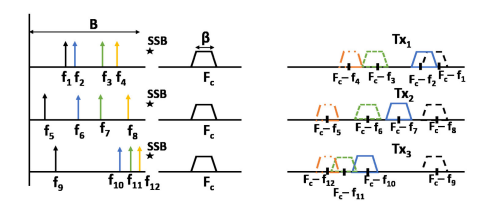


Fig. 3. Spectra of the transmitted signal obtained by Single side-band (SSB) modulation of the chirp waveform with center frequency f_c , and bandwidth β with sinusoidal signals whose frequencies are chosen at random over a frequency range of [0,B] such that each transmitter utilizes 1 modulating tone.

 \otimes represents the Kronecker product and $\bar{\alpha}_{\mathbf{T}}(\xi(\mathbf{i})) \in \mathbb{C}^{N_{\theta} \times N_{\theta}}$ is the diagonal matrix with diagonal elements as the $\xi(n_c)$ transmitter's component of the steering vector for all the angle bins. The individual components are as follows

$$\bar{\mathbf{A}} = \frac{1}{\sqrt{MN_c}} \left[\bar{\mathbf{A}}(0) \quad \cdots \quad \bar{\mathbf{A}}(N-1) \right]$$

$$\bar{\mathbf{A}}(n) = \left[1 \quad \exp\left(-2\pi j \frac{n}{N}\right) \quad \cdots \quad \exp\left(-2\pi j \frac{n(M-1)}{N}\right) \right]^T$$

$$\mathbf{D}_{n_c} = \operatorname{diag} \left[1 \quad \exp\left(-j2\pi \frac{n_c}{N}\right) \quad \cdots \quad \exp\left(-j2\pi \frac{n_c(N-1)}{N}\right) \right]$$

$$\mathbf{H}_{n_c} = \operatorname{diag} \left[1 \quad \exp\left(j2\pi \frac{n_c}{M}\right) \quad \cdots \quad \exp\left(j2\pi \frac{n_c(M-1)}{M}\right) \right]$$
(5)

where $\bar{\mathbf{A}} \in \mathbb{C}^{M \times N}$ are the samples from tones that correspond to each delay bin generated as a result of the de-chirping process in case of a single transmitter and receiver system employing an LFM waveform with bandwidth β Hz, $\mathbf{H}_{n_c} \in \mathbb{C}^{M \times M}$ is the shift in frequency due to the $n_c{}^{th}$ modulating tone, and $\mathbf{D}_{n_c} \in \mathbb{C}^{N \times N}$ contains the phase term associated with different delay bins due to the $n_c{}^{th}$ modulating tone.

Each column of the sensing matrix ${\cal A}$ can be written as

$$\mathcal{A}(n,v) = (\alpha_{\mathbf{R}}(\theta_{\mathbf{v}}) \otimes (\mathbf{E_n} \mathbf{F} \mathbf{G_n})) \,\hat{\mathbf{c}}(v) \tag{6}$$

$$\hat{c}_{n_c}(v) = \hat{c}_{n_c} \alpha_T \left(\theta_v; \xi(n_c)\right) \tag{7}$$

where $n=0,\ldots,N-1,\ v=0,\ldots,N_{\theta}-1.$ The individual terms are

$$\mathbf{E}_n = \operatorname{diag}\left[1 \quad \exp\left(-j2\pi\frac{n}{N}\right) \quad \cdots \quad \exp\left(-j2\pi\frac{n(M-1)}{N}\right)\right]$$

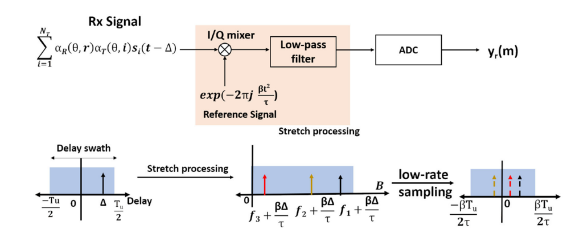


Fig. 4. The figure illustrates the structure of the received signal due to a single scattering center located with range $c\Delta/2$ and angle θ . The stretch processing at the receiver utilizes the transmitted LFM waveform prior to modulation. The effect of this operation recovers the modulating tones, shown in solid lines in the frequency domain, which are further modulated by a complex exponential with a frequency that depends on the range of the scattering center. The sampling rate is set as $F_s = \beta \tau/t_u$, which leads to an aliased spectrum shown in dashed lines

$$\mathbf{F} = \frac{1}{\sqrt{MN_c}} \left[\mathbf{F}(0) \quad \cdots \quad \mathbf{F}(N-1) \right]$$

$$\mathbf{F}(n_c) = \left[1 \quad \exp\left(2\pi j \frac{n_c}{M}\right) \quad \cdots \quad \exp\left(2\pi j \frac{n_c(M-1)}{M}\right) \right]^T,$$

$$\mathbf{G}_n = \operatorname{diag} \left[1 \quad \exp\left(-j2\pi \frac{n}{N}\right) \quad \cdots \quad \exp\left(-j2\pi \frac{n(N-1)}{N}\right) \right],$$

and $\hat{\mathbf{c}}(v) = [\hat{c}_0(v) \cdots \hat{c}_{N-1}(v)]^T \in \mathbb{C}^N$ is the random vector with independent components that selects the modulating waveform.

B. Target Model

We consider the statistical model studied in [44] for the sparse range profile of targets. We assume that the targets are located at the $NN_{\theta}=NN_RN_T$ discrete locations corresponding to different delay bins and angle bins. The support of the K-sparse range profile is chosen uniformly from all possible subsets of size K. The complex amplitude of the non-zero component is assumed to have an arbitrary magnitude and uniformly distributed phase in $[0,2\pi]$. We also empirically study the performance of the proposed illumination system for targets not located on the grid. For the off-grid problem, we assume a minimum separation between the targets in the delay and angle of arrival domain, which is chosen based on the system resolution in each domain. The minimum separation used in the simulation studies for the delay domain is $\min_{i,j} |\Delta_i - \Delta_j| > 2/B$, and the angle of arrival domain is $\min_{i,j} |\cos \theta_i - \cos \theta_j| \geq 2/N_T N_R$.

Clutter Model: The sparsity assumption on the scattering centers is valid for the application problem of surface/naval early warning radar. The radar is typically used in surveying air traffic. The clutter signal is usually stationary in this scenario, which can be separated by coherently integrating across multiple pulses. Simple moving target indication (MTI) processing steps such as 2 pulse or 3 pulse MTI cancellers can be used to suppress stationary clutter [1]. Alternatively, Doppler filtering or Doppler Focusing can be used to separate scattering centers based on Doppler velocity [27]. Further analysis is required on the ambiguity function [72], [73] to establish recovery guarantees, which is robust to the clutter signal component.

C. Problem Statement

Given a sparse scene with targets following the statistical model discussed in previous section, and measurement scheme in (3) with $M \ll NN_{\theta}$ and sparsity level $K \ll NN_{\theta}$, the goal of compressed sensing [74] is to recover the sparse or compressible vector \mathbf{x} using minimum number of measurements in \mathbf{y} constructed using random linear projections \mathbf{A} . The search for the sparsest solution can be formulated as an optimization problem given below $\min_{\mathbf{x}} \|\mathbf{x}\|_0$, subject to $\|\mathbf{A}\mathbf{x} - \mathbf{y}\|_2 \leq \eta$, where η^2 is the noise variance. This problem is NP-hard and hence, intractable as shown in [75], and many approximate solutions have been found. One particular solution is to use the convex relaxation technique to modify the objective as an ℓ_1 norm minimization instead of the non-convex ℓ_0 norm, which is given by,

$$\min_{\mathbf{x}} \|\mathbf{x}\|_1 \text{ subject to } \|\mathbf{A}\mathbf{x} - \mathbf{y}\|_2 \le \eta.$$
 (8)

This approach has been shown to recover sparse or compressible vectors successfully [10], [76] given that the sub-matrices formed by columns of the sensing matrix are well-conditioned. Our analysis is based on LASSO [13], which is a related method that solves the optimization problem in (8). It has been shown in [11] that for an appropriate choice of λ and conditions on measurement matrix are satisfied, then the support of the solution of the below-mentioned optimization problem coincides with the support of the solution of the intractable problem, $\min_{\mathbf{x}} \lambda \|\mathbf{x}\|_1 + \frac{1}{2} \|\mathcal{A}\mathbf{x} - \mathbf{y}\|_2^2$. In this paper, we show that the measurement model formulated in (4) satisfies the conditions on mutual coherence given in [11]. Next, we find a bound on the sparsity level of range profile, which guarantees successful support recovery of almost all sparse signals using LASSO with high probability from noisy measurements. Finally, we also provide an estimate of the number of measurements required for the operator representing our scheme to satisfy the restricted isometry property (RIP) of order K. We consider the space of Ksparse vector $\mathbf{x} \in \mathbb{C}^{NN_{\theta}}$ where $\|\mathbf{x}\|_{2} \leq 1$ denoted by $\mathcal{D}_{K,NN_{\theta}}$. The RIP condition of order K is true if the following condition is true for $\mathbf{x} \in \mathcal{D}_{K,NN_{\theta}}$, $(1 - \delta) \|\mathbf{x}\|_{2}^{2} \leq \|\mathcal{A}\mathbf{x}\|_{2}^{2} \leq (1 + \delta) \|\mathbf{x}\|_{2}^{2}$. Equivalently, the condition can be stated as

$$\delta_K = \sup_{\mathbf{x} \in \mathcal{D}_{K,NN_{\theta}}} \left| \| \mathcal{A} \mathbf{x} \|_2^2 - \| \mathbf{x} \|^2 \right|. \tag{9}$$

In this paper, we bound the random variable δ_K using the theory for bounding stochastic processes [77] adapted to the CS setting in [46], [53]. The next section presents the main results of our analysis.

III. RECOVERY GUARANTEES

The following theorems state the recovery guarantee for the proposed MIMO radar system.

Theorem 1: Consider a compressive MIMO radar system with the measurement model $\mathbf{y} = \mathcal{A}\mathbf{x} + \mathbf{w}$, where $\mathcal{A} \in \mathbb{C}^{N_R M \times N_R N_T N}$ is defined in (4) such that the target scene \mathbf{x} is drawn from a K-sparse model with complex unknown amplitudes and observed in i.i.d. noise process $\mathbf{w} \sim \mathcal{CN}(0, \sigma^2 I)$. The support of the targets in the scene can be recovered using a LASSO estimator with arbitrarily high

probability for a system using M samples at each receiver and $N_c \sim \mathcal{O}(N/N_T)$ tones at each transmitter with $M \sim \mathcal{O}(\log^3(NN_RN_T))$, if the target scene consists of K targets with $K \sim \mathcal{O}(N_RM/\log^2(2\,NN_RN_T))$ of minimum amplitude

$$\min_{k \in \mathbf{S}} |x_k| > \frac{8}{\sqrt{1 - \epsilon}} \sigma \sqrt{2 \log(N N_R N_T)}, \tag{10}$$

As the number of tones employed in modulating the chirp waveform exceeds $N_c \geq 4\log(NN_RN_T + MN_R)/(9N_T)$ shown in Lemma 1 the operator norm of the sensing scheme is bounded with high probability. Furthermore, if the number of tones scales $N_c = \mathcal{O})(\frac{N}{N_T})$, the scaling factor associated with the mutual coherence can be controlled as shown in Lemma 3. The condition on mutual coherence is required for the application of the recovery results in [11].

Theorem 2: For the measurement matrix \mathcal{A} given in (4) and any $\delta \in [0,1]$, the RIP condition in (9) as $\delta_K(\mathcal{A}) \leq \delta$ is satisfied with high probability if the number of measurements M per receiver satisfies the condition $M \geq \delta^{-2} K \log(\frac{N_R N_T N}{K})$

IV. OFF-GRID RECOVERY ALGORITHM

Next, we consider targets that lie in the continuous range and angle-of-arrival domain. The key objective of this section is to analyze the stability of the system to off-grid targets. We evaluate the performance of the system by utilizing an off-grid algorithm proposed in [78]. We evaluate the performance of our proposed system by extending the algorithm We define the parameter space $\Omega = \{(\Delta,\theta)|\Delta\in(0,t_u),\theta\in(-1,1)\}$ The samples at the stretch processor's output at receiver k due to a target with a time of arrival given by Δ and angle of arrival θ as stated in (11). For a scene containing K scattering centers, the measurements are given by

$$\mathbf{y} = \sum_{k=1}^{K} x_k \mathbf{\Psi} \left(\Delta_k, \theta_k \right) + \mathbf{w},$$

$$\Psi\left(\Delta_{k}, \theta_{k}\right) = \sum_{n_{c}=1}^{N} \hat{c}_{n_{c}} \exp\left(-j\phi_{n_{c}}\right) \alpha_{T}\left(\theta_{k}; \xi(n_{c})\right) \boldsymbol{\alpha}_{\boldsymbol{R}}\left(\theta_{k}\right)$$

$$\otimes \exp\left(j2\pi \left[f_{n_c} \left(\frac{\mathbf{m}}{F_s} - \Delta_k \right) + \frac{\beta \Delta_k \mathbf{m}}{\tau F_s} \right] \right)$$
 (11)

where f_{nc} is the frequency of the modulating tone utilized in transmitter v, $\mathbf{w} \sim \mathcal{CN}(0, \sigma_n^2 \mathbf{I})$ is the receiver noise following a complex Gaussian distribution, x_k are the complex scattering coefficients, Δ_k, θ_k are the delay and angle of arrival for each scattering center, $\mathbf{m} = [0, 1, \dots, M-1]$ denote the M time samples at each receiver, and $\mathbf{\Psi}$ is the known structured response parametrized by the time and angle of arrival of the scattering center due to the proposed illumination scheme. We utilize the differentiability of the measurement model in the unknown range of the targets in the scene and adopt the method proposed in [78] to solve the sparse estimation problem in the continuum defined by

$$\min_{\mathbf{x}(\Omega)} \left\| \mathbf{y} - \int_{\Omega} \mathbf{\Psi}(\Omega) dx(\Omega) \right\|^2 \quad \text{ subject to } \left\| \mathbf{x}(\Omega) \right\|_{TV} < \tau,$$

where $\mathbf{x}(\Omega)$ is a sparse discrete measure on the parameter space Ω , $\|\mathbf{x}(\Omega)\|_{TV}$ is the counterpart of ℓ_1 norm over the continuum. Algorithm 1 provides the details of the method used to solve the estimation problem with sparsity constraints. The method first selects the most explanatory choice of parameters in the parameter space using the residual as shown in (12). Next, the weights and the support are refined jointly. This non-convex problem of jointly estimating the weights and the parameters is solved by an alternating minimization approach. The weights are estimated by solving the finite-dimensional problem on the detected support set by enforcing the ℓ_1 constraint on the weights. The support set is pruned such that only non-zero points in the support set are retained. Next, the support set is refined using the gradient information with the steepest descent method with line search. We consider the convergence condition as a combination of the residual error and the reduction in the loss function.

Algorithm 1: Alternating descent conditional gradient method [78].

```
Input: \mathbf{y}, \tau, \Psi, \nabla_{\Theta \in \Omega} \Psi, \Omega, and K_{max}.
Return: complex weights x, delay and angle of arrival of
 scattering centers \{\theta, \Delta\} \in \Omega.
Initialize k = 0, support set S = \{\emptyset\}
while (Convergence condition is not satisfied or
 k \leq K_{max}
  Residual: \mathbf{r}_k = \mathbf{y} - \sum_{k=1}^{k-1} \mathbf{\Psi}(\Delta_k, \theta_k) x_k,
  Gradient of loss function: \mathbf{g}_k(\mathbf{r}_k) = \nabla_{\mathbf{r}} \left(0.5 \|\mathbf{r}_k\|_2^2\right)
   \{\Delta_{k}, \theta_{k}\} = \arg \max_{\{\Delta, \theta\} \in \Omega} |\langle \Psi(\Delta, \theta), \mathbf{g}_{k} \rangle|,
  S = S \bigcup \{\Delta_k, \theta_k\}
                                                                                          (12)
      while (Convergence condition)
        Compute weights: \arg\min_{\|\mathbf{x}\|_1 \leq \tau}^{\mathbf{x}} \|\mathbf{\Psi}_S \mathbf{x} - \mathbf{y}\|^2
        Prune Support: If |x_k| = 0 S = S \setminus \{\Delta_k, \theta_k\}
        Refine support: S = S - \nabla_S \|\mathbf{\Psi}_S \mathbf{x} - \mathbf{y}\|^2
      end
      k = |S|
end
```

Convergence analysis and complexity: The optimization procedure has a sub-linear rate of convergence as shown in [78], [79], such that the number of iterations is given by $\mathcal{O}(1/\bar{\epsilon})$, where $\bar{\epsilon}$ refers to the required error tolerance. This guarantee is slower compared to the $\mathcal{O}(1/\sqrt{\bar{\epsilon}})$ for on-grid algorithms such as Fast iterative shrinkage-thresholding algorithm (FISTA) [80]. An alternative method that formulates the off-grid sparse estimation problem using particles and gradient-descent has been proposed in [81]. Although the proposed method has local linear convergence given by $\mathcal{O}(\log(1/\bar{\epsilon}))$ but the problem is still non-convex and further analysis is required for stability to additive noise. More recently, data-driven models [18]–[20]

that unroll the optimization iterations. These methods also have linear convergence rates given by $\mathcal{O}(\log(1/\bar{\epsilon}))$ but the stability to off-grid targets is not investigated. The fundamental resolution of the system is controlled by the Rayleigh length, which is a function of the system parameters such as bandwidth, total array aperture length [82]. The super-resolution of targets are typically achieved by over-discretizing the search grid and utilizing the Rayleigh length to obtain efficient numerical algorithms [83]. Additionally, prior information on the non-zero locations in the search space has been utilized to super-resolve target locations using reweighted methods [84]–[86] that iteratively refine the parameter estimates. These numerical techniques can be utilized with our measurements using the forward-operator to super-resolve targets iteratively.

V. SIMULATION RESULTS

In this section we conduct simulation studies to study the performance of the proposed compressive radar sensor as a function of system parameters. Fixed parameters of the simulations are Bandwidth B=500 MHz, unambiguous range Interval [0,100]m, Number of Range Bins N=334 and pulse duration $\tau=6.86\times 10^{-5}s$.

A. Effect of Multi-Tones on Mutual Coherence

We first study increasing the number of tones in a single transmitter and receiver. We compare the proposed illumination scheme with a uniformly sub-sampled Toeplitz matrix with independent and identical elements sampled from a complex standard normal distribution. The Toeplitz sensing matrix represents the impulse response of the linear time-invariant system with a randomly distributed waveform with independent entries as input. We also compare it with the mutual coherence of Xampling based sub-Nyquist radar that utilizes Direct Fast Fourier transform (FFT) sampling presented in [27] described by the equation (15) for range estimation. The bandwidth of each sub-band is 25 MHz. The frequency-agile radar [38] is also compared for both range estimation and range-Doppler velocity estimation. The forward operator used is derived from 16 in [38]. We compare the mutual coherence with the range dictionary, assuming the doppler bin is known as apriori and the mutual coherence for the joint range and Doppler velocity dictionary. From Fig. 5(a), we observe that the coherence of a system employing a single tone is high for lower sampling rates. Increasing the number of tones improves the mutual coherence as the number of modulating tones increases, the mutual coherence of the system converges in mean to the mutual coherence of structured random Toeplitz matrix. The mutual coherence of the Xampling based sub-Nyquist radar and we observe that for smaller sub-sampling factor $\frac{B}{B}$ < 0.5 has higher mutual coherence compared to our system because of the structured block-wise Fourier samples. When the Doppler velocity is known, the frequency-agile radar has a similar mutual coherence as the non-uniformly sampled Fourier operator. For the case of unknown range-doppler, the measurement operator has a similar mutual coherence to our waveform.

Next, we compare the coherence of the proposed system with a multiple-input system with a single receiver employing samples from a Gaussian distribution, which leads to a partial block

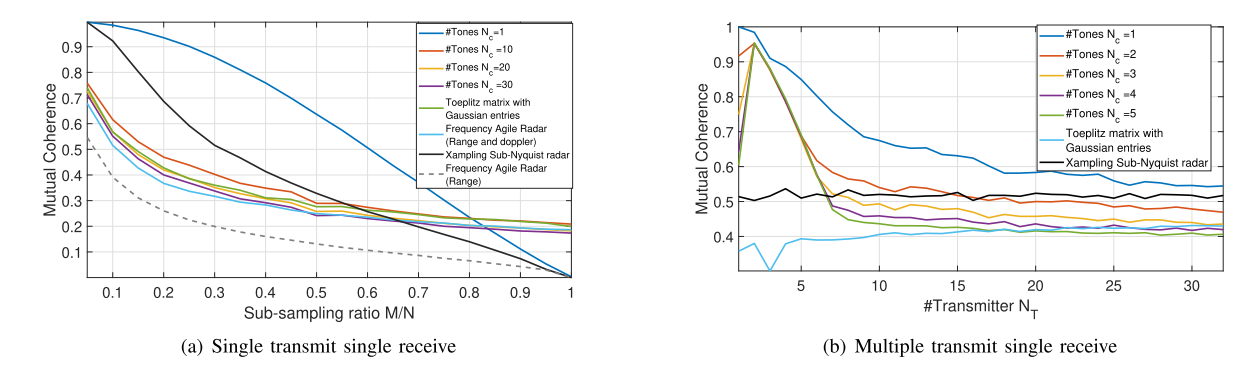


Fig. 5. Fig. 5(a) illustrates the mutual coherence of a single transmit and a single receiver system as a function of sub-sampling ratio $\frac{\beta}{B}=M/N$ as the number of chirps N_c is increased along with the mutual coherence of the uniformly sub-sampled random Toeplitz matrix, Sub-Nyquist radar system based on Xampling [27] and the frequency agile radar utilizing randomized frequency step [38]. Fig. 5(b) illustrates the mutual coherence of multiple transmit system with single receiver as a function of number of transmitters N_T as number of chirps N_c is increased along with the mutual coherence of the random block Toeplitz matrix and the sub-Nyquist radar applied to a multiple transmit and single receive radar system [31]. The under-sampling ratio M/N is set as 0.3.

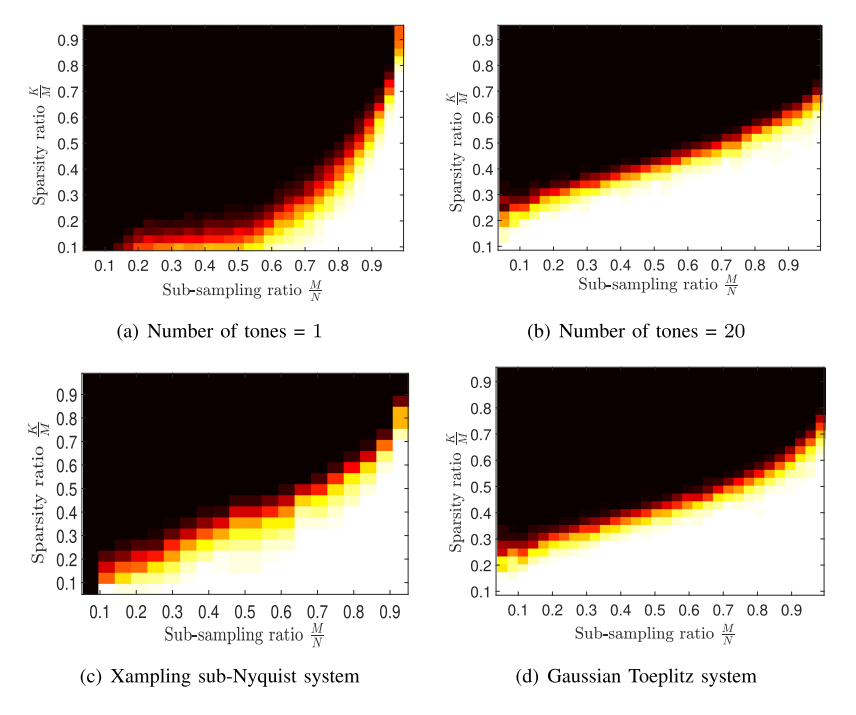
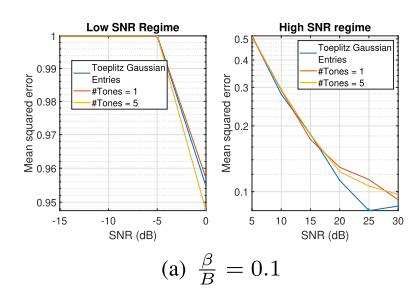


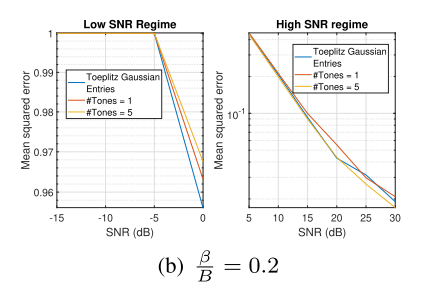
Fig. 6. Fig. 6(a), 6(b) illustrate the probability of reconstruction error is below 10^{-5} in the noiseless setting as a function of sub-sampling and sparsity ratio for the multi-tone LFM system. Fig. 6(d) shows the performance for the system employing Gaussian samples as waveform and Fig. 6(c) illustrates.

Toeplitz measurement matrix with random Gaussian entries. We fix the sub-sampling factor of $\frac{\beta}{B} = \frac{M}{N} = 0.3$ to assess the mutual coherence as the number of transmitters grows. From Fig. 5(b), we can see that as the number of transmitters and modulating tones increase, the randomness in the waveform increases, and hence the mutual coherence of the system approaches that of a system employing random waveform with independent samples from the Gaussian distribution. We also compare the mutual coherence with Sub-Nyquist radar [31] operating in Mode 1 such that there is no spatial compression. Our prosed system has a lower mutual coherence than the Xampling system as the number of tones utilized per transmitter increases for the range and angle of arrival estimation.

B. On-Grid Recovery

Estimation performance: In this section, we consider a single transmit/receive system and evaluate the ability of the system to estimate the scattering coefficients using Mean squared error as the performance criterion. First, we consider the noiseless case and evaluate the performance of the proposed waveform, a system employing a waveform with Gaussian entries denoted by the Toeplitz matrix and a sub-Nyquist based radar system reconstruction error as a performance criterion. In Figs. 6(a) 6(b), 6(c), 6(d) the probability of successful recovery (defined as reconstruction error $< 10^{-5}$) is shown as a function of sparsity ratio (the ratio of number of targets in the scene to number of measurements $\frac{K}{M}$) and sub-sampling ratio ($\frac{\beta}{B} = \frac{M}{N}$). We





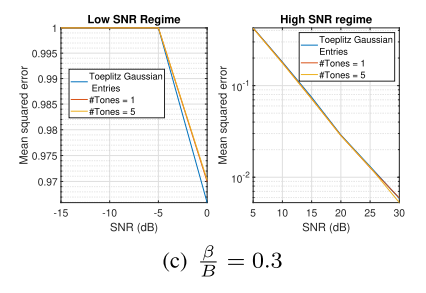


Fig. 7. Fig. 7(a),7(b) and 7(c) illustrate the mean squared error as a function of the signal to noise ratio (SNR) for different sub-sampling factors of $\frac{\beta}{B} = 0.1, 0.2, 0.3$, respectively with number of transmitters $N_T = 16$, and number of receivers $N_R = 8$. The sparsity ratio of the scene is fixed at $\frac{K}{M} = 0.1$ for these simulations.

observe that for a sufficiently high number of modulating tones, the performance characterized by the phase transition diagram 6 is similar to that of a system employing stochastic waveforms on transmit. Furthermore, we also show that as the number of modulating tones increases, our system can recover the scattering coefficients of the targets at a higher sparsity ratio for each sub-sampling ratio $\frac{\beta}{B} < 0.5$ compared to the sub-Nyquist radar system.

Next, we consider a multiple transmit/ receive system with $N_T=16$ and $N_R=8$ to evaluate the performance of our proposed system and a system that utilizes samples from a Gaussian distribution modeled as a block-Toeplitz matrix used for estimating the scattering coefficients in range-angle of arrival domain. We denote the Signal to noise ratio measure as the post-integration SNR after the stretch processing step, which is the analog domain approximation of the matched filtering. The SNR relationship is given by

$$\begin{split} SNR(dB) &= 10 \log_{10} S_{Power} - 10 \log_{10} N_{Power} \\ &+ 10 \log_{10} P_{Stretch}, \end{split}$$

where the signal power is governed by the Radar range equation, noise power is governed by the system bandwidth and the stretch processing gain dependes on the bandwidth-time product of the LFM waveform, which can be stated as

$$S_{Power} = \frac{P_{Trans}G_{Trans}G_{Rec}\lambda^2\sigma_{RCS}}{(4\pi)^3R_{scene}^4},$$

$$N_{Power} = k_{Boltzman}B/2T,$$

$$P_{Stretch} = \beta\tau,$$

where P_{Trans} is the peak transmitted power, G_{Trans}, G_{Rec} are the transmit and receive antenna gain, σ_{RCS} is the radar cross section of the target and R_{scene} is the distance between the radar platform and the scene center. For the choice of parameters with $P_{Trans}=10$ KW, and $G_{Trans}(dB)=20\,dB, G_{Rec}(dB)=20\,dB$ and $\sigma_{RCS}=1$ and R=10000 m, we get an $SNR=15\,dB$. We vary the SNR for a fixed sparsity ratio of $\frac{K}{M}=0.1$ and compare the system performance for subsampling ratio of $\frac{\beta}{B}=0.1,0.2,0.3$ in Fig. 7. We observe that for the High SNR regime where $SNR>5\,dB$ the performance of the MIMO system with $N_c=1$ modulating tone per transmitter converges to the MIMO system with Gaussian samples. For low SNR regime $SNR<5\,dB$, the performance improves as the number of modulating tones per transmitter increases.

Detection performance: Next, we consider noisy measurements to assess the system's performance and compare it with a system utilizing a waveform with Gaussian samples. We first consider a single transmit/receive system and fix the under-sampling ratio to 0.3. Support recovery performance is evaluated using the probability of detection and false alarm. The detection is declared true if the recovered signal at a bin exceeds the threshold and the target is present at the specified location. All other detections are declared as false positives. The receiver operating characteristics (ROC) curve illustrates the probability of detection and false alarm parametrized by the threshold. We characterize the performance criterion for successful support recovery (defined by the area under the curve (AUC) of ROC exceeding a threshold of 0.99) as a function of the signal-to-noise ratio (SNR) and sparsity ratio $\frac{K}{M}$. The results in Figs. 8(a) to 8(d) illustrate that the successful recovery of the system improves as the number of tones N_c increases and converges to the system with Gaussian samples represented by a Toeplitz matrix. Next, we fix the SNR as 10 dB and study the criterion for support recovery (defined by the area under ROC (AUC) exceeding a threshold of 0.9) as the sub-sampling ratio sparsity levels are varied. The probability of successful recovery is shown in Figs. 9(a) to 9(d). It can be seen that the performance of the system approaches the performance of the system employing waveform with Gaussian samples. Next, we characterize the performance of the MIMO system for support recovery using the Receiver operating characteristics for successful support recovery in Fig. 10. We fix the sparsity level of the scene to $\frac{K}{M} = 0.3$ and consider a MIMO system with $N_T = 16$ transmitters and $N_R = 8$ receivers and vary the number of modulating tones per transmitter. We set the sub-sampling ratio as M/N = 0.1, 0.2, 0.3 in Fig. 10(a), 10(b), and 10(c), respectively. We vary the SNR and compare the AUC for ROC curve for a system employing random waveform with samples from a Gaussian distribution. We show that by utilizing $N_c = 1$ tone per transmitter, the performance of the proposed MIMO system converges to the performance of the MIMO system with Gaussian waveform. We further show the effect of noise variance on the support recovery guarantee in the form of a phase transition diagram in Fig. 11, where the criterion used is even that the area under the ROC curve exceeds AUC > 0.95. We utilize a sub-sampling factor of $\frac{\beta}{B} = \frac{M}{N} = 0.3$. Again, we observe that a system utilizing a single modulating tone per transmitter can achieve similar performance to a MIMO system that employs Gaussian waveform.

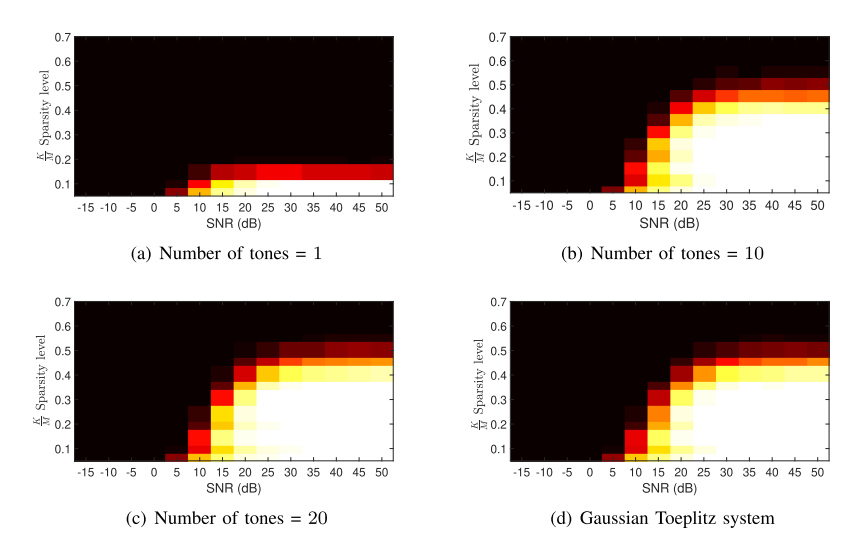


Fig. 8. Fig. 8(a) to 8(d) shows the probability that Area under the curve for Receiver operating characteristic > 0.95 as a function of signal to noise ratio at a fixed under-sampling ratio $\beta/B = 0.3$.

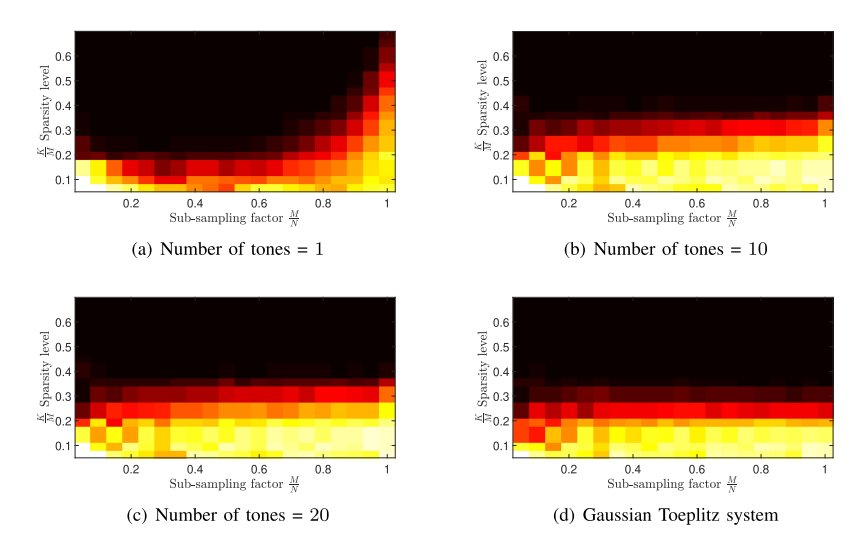


Fig. 9. Fig. 9(a) to 9(d) shows the probability that AUC \geq 0.9 as a function of sub-sampling ratio $\beta/B=M/N$ for a fixed SNR of 10~dB.

C. Off-Grid Recovery

We consider a single input single output system for estimating the range and evaluate the performance of the illumination scheme with off-grid targets. We conduct the simulations with an under-sampling ratio as $\frac{M}{N} = 1/3$ and the SNR of 12 dB. The number of targets in the scene is 20 using the model specified in section II-B. We compare the performance of the system as the number of modulating tones is varied using the metrics defined in [87]. We define the set of true range as $\mathcal{T} = \{r_i\} \subset \Omega$ with complex scattering coefficients $\{x_i\}$ for $i = 1, \dots, K$, where Kis the number of targets in the scene. We define N_{r_i} as the set of values of range that are in a neighborhood of the true range r_i , such that $N_{r_i} = \{r : |r - r_i| \le 0.2c/(2B)\}$. We define the region of false detections as $\mathcal{F} = \Omega \setminus \{ \cup_i N_{r_i} \}$. We consider the following performance measures to evaluate the estimate $\{\hat{r}_i\}$, and $\{\hat{x}_i\}$ obtained using the algorithm given by

• error due to false detections given by $m_1 = \sum_{\hat{r}_i \in \mathcal{F}} |\hat{x}_i|$,

- weighted localization $m_2 =$ $\sum_{j} \sum_{i: \hat{r}_i \in N_{r_j}} |\hat{x}_i| \min_{r \in \mathcal{T}} ||\hat{r}_i - r||^2,$ • approximation error in the scattering coefficients $m_3 =$
- $\max_{j} |x_j \sum_{l:\hat{r}_l \in N_{r_i}} \hat{x}_l|.$

First, we evaluate the resolution performance of the system using 2 targets with ranges R_1 and R_2 . The scattering coefficients are chosen at random from a Complex Gaussian distribution. The SNR is set as 12 dB. We set the sub-sampling ratio $\frac{B}{B} = 0.3$. The distance between the target is increased and we measure the estimation error for each target denoted by $Error = |R_1 - \hat{R}_1| + |R_2 - \hat{R}_2|$. We observe in Fig. 13 that as the number of tones $N_c = 1, 5, 10$. As the number of tones increases the error reduces. We observe that the for $N_c = 10$, the error saturates after 0.25 m. The theoretical resolution is $\frac{c}{2B} = 0.3$ m. We evaluate the performance profile, which is studied in [87] to compare the various algorithms for recovery. In our case, we compare the system's performance for a fixed recovery

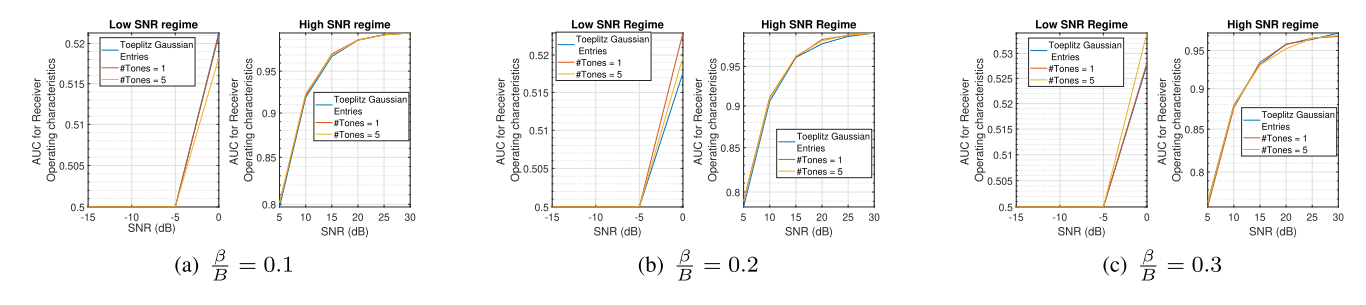


Fig. 10. The number of transmitters $N_T=16$, and the number of receivers is $N_R=8$. The sparsity ratio is set as by $\frac{K}{M}=0.3$. Receiver operating characteristics with the sub-sampling factor of $\frac{\beta}{B}=0.1,0.2,0.3$ in Fig. 10(a) to 10(c).

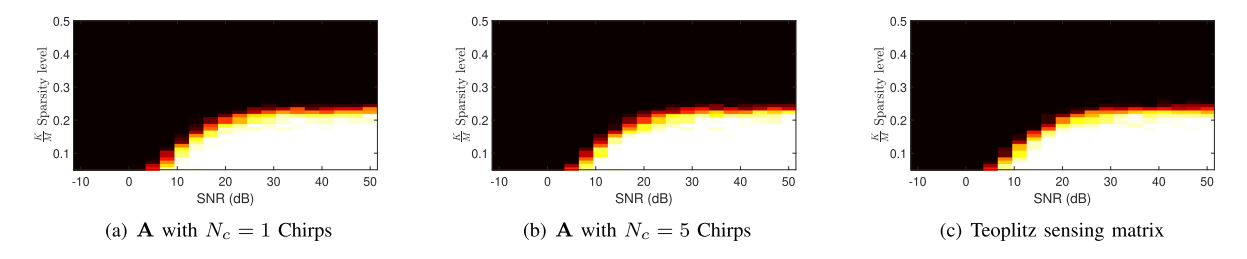


Fig. 11. The sub-sampling ratio is set as M/N=1/3. The number of transmitters and receivers in the system are $N_T=16$, and $N_R=8$, respectively. The probability that AUC under ROC ≥ 0.95 is shown in for the case of system with $N_c=1,5$ and Gaussian waveform in Figs. 11(a), 11(b), and 11(c), respectively.

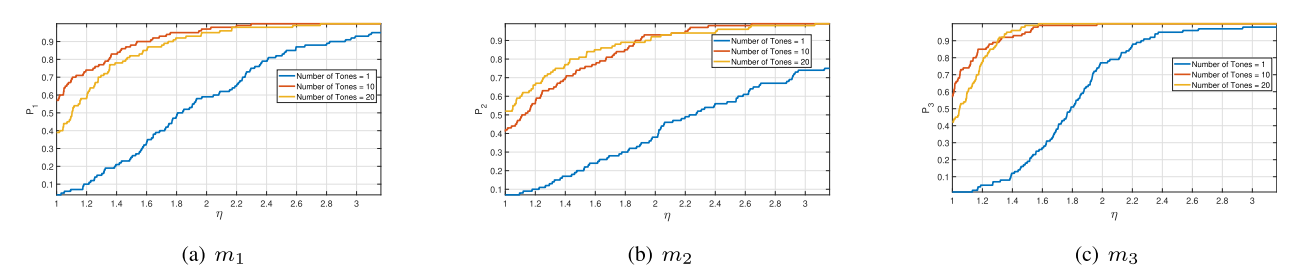


Fig. 12. Performance profile for different number of modulating tones with under-sampling ratio $\beta/B = 1/3$, K = 20 and SNR = 12 dB. Figs. 12(a), 12(b), and 12(c) show the performance profile corresponding to metrics indicating the false positives, localization error, and approximation error, respectively.

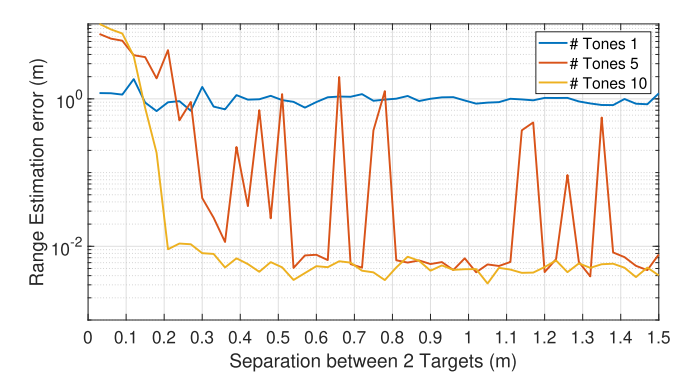


Fig. 13. The resolution of system is verified using Twotargets with varying separation. A single transmit/receive system $N_c=1,5,10$ modulating tones is utilized with SNR=12 dB and sub-sampling ratio $\frac{\beta}{B}=0.3$.

algorithm and vary the number of modulating tones. The set of tones used is denoted by $S = \{1, 10, 20\}$. The performance profile is evaluated by repeating the experiment for different realizations of target denoted by the set P. The performance profile for the system parameter $s \in S$, error metric m_i , and

factor η , which specifies the ratio $m_i(p,s)/\min_s m_i(p,s)$ is computed as follows

$$P_s(\eta; i) = \frac{\operatorname{\mathbf{card}} \left\{ p \in \mathcal{P} : m_i(p, s) \le \eta \min_s m_i(p, s) \right\}}{\operatorname{\mathbf{card}} \left\{ \mathcal{P} \right\}}.$$

The performance profile of system s indicates the number of realizations such that the error metric $m_i(p,s)$ for the realization p is within a factor of β from the error metric corresponding to the best system parameter. Fig. 12 shows the profile evaluated for all the error metrics computed using 100 target realizations. We observe that as the number of modulating tones is increased, the performance improves.

VI. PROOFS

We estimate the tail bounds for mutual coherence and spectral or operator norm of the measurement matrix to obtain the non-asymptotic recovery guarantee for our system. We make use of the Matrix Bernstein inequality to bound the operator norm of the measurement matrix with high probability given in (4). Complete proofs are presented in [88] and the supplementary material.

Lemma 1: The operator norm of the sensing matrix in (4) is bounded with high probability if $N_c \ge 4\log(NN_RN_T + MN_R)/(9N_T)$

$$\|\mathbf{A}\|_{op} \le 2\sqrt{\frac{N_T N}{M} \log\left(N_R M + N_R N_T N\right)}.$$
 (13)

The following results on the Euclidean norm of columns and the mutual coherence are obtained using concentration inequalities for quadratic forms of random vectors having a sub-Gaussian distribution given in [89].

Lemma 2: The minimum of the corollary-Euclidean norm of any column of \mathcal{A} , which is indexed by range bin n angle bin v is bounded by

$$\left| \min_{n,v} \left\| \mathcal{A}(n,v) \right\|_2^2 - 1 \right| \le \epsilon \tag{14}$$

with high probability, where $\epsilon \in (0,1)$ is an arbitrary constant. Lemma 3: The mutual coherence of the sensing matrix ${\cal A}$ scales as

$$\mu\left(\mathcal{A}\right) \sim \mathcal{O}\left(\sqrt{\frac{\log(\frac{NN_RN_T}{\epsilon})}{M}}\right),$$
 (15)

with high probability if $N_c = \mathcal{O}(\frac{N}{N_T})$.

Proof of Theorem 1: Using $M \ge \log(NN_RN_T)^3$ from lemma 3, the coherence condition given in [11] is satisfied with high probability as shown below

$$\mu\left(\mathcal{A}\right) = \mathcal{O}\left(\frac{1}{\log(NN_RN_T)}\right)$$
w.p. $p_1 \ge 1 - \epsilon - 10 N \exp\left(-dM\bar{\epsilon}^2\right)$, (16)

where $\bar{\epsilon}=(\epsilon\frac{q^*}{(\frac{N_cN_T}{N})^{\frac{2}{q^*}-1}}), \epsilon\in(0,1).$ The measurement matrix

in our analysis is normalized to have unit norm columns to apply results from [11]. Let $\mathbf{D} \in \mathbb{R}^{N_R N_T N \times N_R N_T N}$ diagonal matrix with diagonal entries corresponding to the norm of the column of \mathcal{A} given by $D_{i,i} = \|\mathcal{A}(n_i, v_i)\|_2$. The measurement model can be modified as $\mathbf{y} = \hat{\mathcal{A}}\mathbf{z} + \mathbf{w}$, where $\hat{\mathcal{A}} = \mathcal{A}\mathbf{D}^{-1}$ and $\mathbf{z} = \mathbf{D}\mathbf{x}$. Next, we obtain the probability tail bound for the operator norm of the measurement matrix $\hat{\mathcal{A}}$. Using 1, we have $\forall \epsilon > 0, \epsilon \in (0,1)$, independent of N and M,

$$\begin{split} &P\left(\left\|\hat{\mathcal{A}}\right\|_{op} \geq \frac{2}{\sqrt{1-\epsilon}}\sqrt{\frac{N_TN}{M}}\log\left(N_RM + N_RN_TN\right)\right) \\ &\leq \left(\frac{1}{N_RM + N_TN_RN}\right)^{\alpha_1-1} + 8N\exp\left(-dM\bar{\epsilon}^2\right), \end{split}$$

where

$$\begin{split} \alpha_1 &= \frac{1}{\frac{1}{3}\sqrt{\frac{1}{N_T N_C}\log\left(N_R M + N_R N_T N\right)} + \frac{1}{2}},\\ N_c N_T &\geq \frac{4}{9}\log(NN_R N_T + MN_R), \bar{\epsilon} = \left(\epsilon \frac{q^*}{\left(\frac{N_c N_T}{N_C}\right)^{\frac{2}{q^*} - 1}}\right). \end{split}$$

Therefore,

$$\begin{split} \left\| \hat{\mathcal{A}} \right\|_{op} &\leq \frac{2}{\sqrt{1 - \epsilon}} \sqrt{\frac{N_T N}{M} \log \left(N_R M + N_R N_T N \right)} \\ \text{w.p. } p_2 &\geq 1 - \left(\frac{1}{N_R M + N_T N_R N} \right)^{\alpha_1 - 1} \\ &+ 8 N \exp \left(-dM \bar{\epsilon}^2 \right). \end{split} \tag{17}$$

Using the support recovery result from [11], the maximum number of targets that can be successfully detected is $K_{max} = \frac{c_0 N_R M}{\log^2(NN_R N_T + MN_R)}$. Next, we establish that the measurement matrix does not reduce the absolute value of non-zero entries of the sparse vector \mathbf{x} below the noise level.

$$P\left(\min_{i} D_{i,i} | x_{i} | \leq 8\sigma \sqrt{2 \log N}\right) \leq NP\left(D_{i,i} \leq \sqrt{1 - \epsilon}\right)$$

$$\leq 8 N \exp\left(-dM\bar{\epsilon}^{2}\right).$$

Therefore, we have

$$\min_{i} |z_{i}| \ge 8\sigma \sqrt{2\log N}$$
w.p. $p_{3} > 1 - 8N \exp\left(-dM\bar{\epsilon}^{2}\right)$. (18)

We define the following events associated with a realization of measurement matrix A

$$\Xi_{1}: \mu\left(\mathbf{A}\right) = \mathcal{O}\left(\frac{1}{\log N}\right), \Xi_{2}: \left\|\hat{\mathbf{A}}\right\|_{op}^{2} \leq \frac{c_{0} N}{K_{\max} \log N},$$
$$\Xi_{3}: \min_{i} |z_{i}| \geq 8\sigma \sqrt{2 \log N},$$

 Ξ_4 : successful support recovery for a fixed sensing matrix.

Let Ξ be the event that the sampled measurement matrix satisfies the conditions required for successful recovery and recovers a K-sparse vector \mathbf{x} selected from the target model. This implies

$$P\left(\Xi\right) \ge P\left(\Xi_4 \mid \Xi_1 \cap \Xi_2 \cap \Xi_3\right)$$

$$\left(1 - P\left(\Xi_1^c\right) - P\left(\Xi_2^c\right) - P\left(\Xi_3^c\right)\right). \tag{19}$$

Using result from [11] for $P(\Xi_4 \mid \Xi_1 \cap \Xi_2 \cap \Xi_3)$,(17), (18) and (16) in (19), we deduce that successful support recovery is guaranteed with high probability.

The conditions required for RIP of order K to hold are obtained next. We reformulate the system model presented in (3) and (4) by re-scaling the random variables to normalize the variance as follows

$$\mathcal{A} = \sum_{n_c=1}^{N} \hat{c}_{n_c} \sqrt{\frac{N_c N_T}{N}} \left(\bar{\alpha}_{\mathbf{R}} \bar{\alpha}_{\mathbf{T}} (\xi(\mathbf{n_c})) \right) \otimes \left(\mathbf{H}_{n_c} \bar{\mathbf{A}} \mathbf{D}_{n_c} \right),$$

$$\mathcal{A} = \sum_{n_c=1}^{N} c_{n_c} \mathcal{A}_{n_c},$$

$$\mathcal{A}_{\mathbf{n_c}} = \sqrt{\frac{N_c N_T}{N}} \left(\bar{\alpha}_{\mathbf{R}} \bar{\alpha}_{\mathbf{T}} (\xi(\mathbf{n_c})) \right) \otimes \left(\mathbf{H}_{n_c} \bar{\mathbf{A}} \mathbf{D}_{n_c} \right)$$

where $c_{n_c}=\sqrt{\frac{N}{N_cN_T}}\hat{c}_{n_c}$ such that $E(|c_{n_c}|^2)=1.$ We define the set

$$\mathcal{D}_{\mathbf{K}, \mathbf{NN}_{\theta}} = \left\{ \mathbf{x} \in \mathbb{C}^{NN_{\theta}} : \|\mathbf{x}\|_{0} = K, \|\mathbf{x}\|_{2}^{2} \le 1 \right\}.$$

For a K-sparse vector $\mathbf{x} \in \mathcal{D}_{\mathbf{K}, \mathbf{NN}_{\theta}}$, we have

$$\mathbf{A}\mathbf{x} = \mathbf{V}_x \mathbf{c}$$

where $\mathbf{V}_x = [\mathbf{A_1}x \ \mathbf{A_2}x \ \cdots \ \mathbf{A_N}x] \in \mathbb{C}^{MN_R \times N}$ and $\mathbf{c} \in \mathbb{C}^N$ is the vector comprised of the normalized random variables that select the waveforms.

Lemma 4: Given the measurement operator \mathcal{A} and any $\mathbf{x} \in \mathcal{D}_{K,NN_{\theta}}$ we have $\mathbf{E}(\|\mathcal{A}\mathbf{x}\|^2) = \|\mathbf{x}\|^2$.

Lemma 4 implies that the RIP constant of order K in (9) can be expressed as a second order chaos process in the random vector \mathbf{c} as follows

$$\delta_{K} = \sup_{\mathbf{x} \in \mathcal{D}_{K,NN_{\theta}}} \left| \| \mathcal{A} \mathbf{x} \|_{2}^{2} - \| \mathbf{x} \|_{2}^{2} \right|$$

$$= \sup_{\mathbf{x} \in \mathcal{D}_{K,NN_{\theta}}} \left| \| \mathbf{V}_{x} \mathbf{c} \|_{2}^{2} - \mathbf{E} \left(\| \mathbf{V}_{x} \mathbf{c} \|_{2}^{2} \right) \right|. \tag{20}$$

Therefore, we derive the concentration inequality for the RIP constant using the result in Theorem 3, which was first established in [53]. We define the following terms that are essential components in the result

$$\begin{split} & \mathbb{T} = \left\{ \mathbf{V}_{\mathbf{x}} = \left[\mathbf{\mathcal{A}}_{1} \boldsymbol{x} \cdots \mathbf{\mathcal{A}}_{N} \boldsymbol{x} \right] : \mathbf{x} \in \mathcal{D}_{K,NN_{\theta}} \right\}, \\ & d_{F}(\mathbb{T}) = \sup_{\mathbf{V}_{\mathbf{x}} \in \mathbb{T}} \| \mathbf{V}_{\mathbf{x}} \|_{F}, \quad d_{op}(\mathbb{T}) = \sup_{\mathbf{V}_{\mathbf{x}} \in \mathbb{T}} \| \mathbf{V}_{\mathbf{x}} \|_{op}, \\ & \gamma_{2} \left(\mathbb{T}, \|.\|_{op} \right) \leq C \int_{0}^{d_{op}(\mathbb{T})} \sqrt{\log \left(\mathbf{N} \left(\mathbb{T}, \|.\|_{op}, u \right) \right)} du, \end{split}$$

where $\gamma_2(\mathbb{T},\|.\|_{op})$ is the Talgrand's chaining functional, which is upper bounded by Dudley's entropy integral [53], $\mathbf{N}(\mathbb{T},\|.\|_{op},u)$ is the covering number, which is defined by the number of balls with distance metric $\|.\|_{op}$ and radius u required to cover the set of matrices \mathbb{T} induced by the vector $\mathbf{x} \in \mathcal{D}_{K,NN_{\theta}},$ C>0 is a universal constant, and $\log(\mathbf{N}(\mathbb{T},\|.\|_{op},u))$ is defined as the metric entropy. The following lemma derives the estimates for the above defined quantities.

Lemma 5: For the set of matrices \mathbb{T} , we have $d_F(\mathbb{T}) = 1$, $d_{op}(\mathbb{T}) \leq \sqrt{\frac{K}{M}}$, $\gamma_2(\mathbb{T}, \|.\|_{op}) \leq C_1 \sqrt{\frac{K}{M}} (\sqrt{\log(\frac{eNN_{\theta}}{K})})$, for some universal constant $C_1 > 0$.

Theorem 3: Let $\mathbb{T} = \{\mathbf{V}_{\mathbf{x}} : \mathbf{x} \in \mathcal{D}_{K,NN_{\theta}}\}$ be a set of matrices, and let \mathbf{c} be a random vector whose entries c_j are independent, mean-zero, variance 1, and L-subgaussian random variables. Set $E = \gamma_2(\mathbb{T}, \|.\|_{op})(\gamma_2(\mathbb{T}, \|.\|_{op}) + d_F(\mathbb{T})) + d_F(\mathbb{T})d_{op}(\mathbb{T}),$ $V = d_{op}(\mathbb{T})(\gamma_2(\mathbb{T}, \|.\|_{op}) + d_F(\mathbb{T})), \quad U = d_{op}^2(\mathbb{T}).$ Then for t > 0, $P(\sup_{\mathbf{V}_{\mathbf{x}} \in \mathbb{T}} ||\mathbf{V}_{\mathbf{x}} \mathbf{c}||_2^2 - \mathbf{E}(||\mathbf{V}_{\mathbf{x}} \mathbf{c}||_2^2)| > \epsilon_1 E + t)$ $\leq \exp(-\epsilon_2 \min(\frac{t^2}{V^2}, \frac{t}{U})).$ The constants ϵ_1 , ϵ_2 depend only on L.

Proof is given in Theorem 3.2 in [53].

Proof of Theorem 2: Let the restricted isometry constant of order K be δ_K for the measurement operator, which is obtained in (20). We can obtain the tail bounds on δ_K using the results

from Lemma 5 in Theorem 3 as follows

$$P\left(\delta_{K} \geq \epsilon_{1}E + t\right)$$

$$= P\left(\sup_{\mathbf{x} \in \mathcal{D}_{K,NN_{\theta}}} \left| \|\mathbf{V}_{x}\mathbf{c}\|_{2}^{2} - \mathbf{E}\left(\|\mathbf{V}_{\mathbf{x}}\mathbf{c}\|_{2}^{2}\right) \right| \geq \epsilon_{1}E + t\right)$$

$$\leq \exp\left(-\epsilon_{2}\min\left(\frac{t^{2}}{V^{2}}, \frac{t}{U}\right)\right) \leq \eta_{1},$$

where $\epsilon_1, \epsilon_2, E, U, V$ are defined in Theorem 3, and $\eta_1 \in [0, 1]$ is a bound on the tail probability. The constants E, U, V for the measurement operator is given by

$$E \leq C_1^2 \frac{K}{M} \left(\log \left(\frac{eNN_{\theta}}{K} \right) \right) + C_1 \sqrt{\frac{K}{M}} \left(\sqrt{\log \left(\frac{eNN_{\theta}}{K} \right)} \right)$$

$$+ \sqrt{\frac{K}{M}}$$

$$\leq C_2^2 \frac{K}{M} \left(\log \left(\frac{eNN_{\theta}}{K} \right) \right) + C_2 \sqrt{\frac{K}{M}} \left(\sqrt{\log \left(\frac{eNN_{\theta}}{K} \right)} \right)$$

If the number of measurements per receiver $M>2\frac{C_2^2\delta^2}{\epsilon_1^2}K\log(\frac{\epsilon NN_\theta}{K})$, then $E\leq \frac{\delta^2}{4\epsilon_1^2}+\frac{\delta}{2\epsilon_1}\leq \frac{c\delta}{2\epsilon_1}$. Given the condition on the number of measurements, the RIP constant δ_K is bounded as follows using $t=\frac{\delta}{2}$

$$P\left(\delta_{K} \ge \epsilon_{1}E + t\right) = P\left(\delta_{K} \ge \delta\right)$$

$$\le \exp\left(-\frac{\epsilon_{2}}{4} \left(\frac{M^{2} \log\left(\frac{eNN_{\theta}}{K}\right)}{K^{2}} \delta^{2}\right)\right)$$

This relation establishes the condition the number of measurements required per receiver M for the constant δ_K to be bounded with high probability.

VII. CONCLUSION

In this work, we have presented a compressive acquisition scheme for high-resolution radar sensing. We show that the proposed system comprising multi-tone LFM transmit waveforms and uniformly subsampled stretch processor results in a structured random sensing matrix with provable recovery guarantees for delay and angle of arrival estimation in sparse scenes. The recovery guarantees for the proposed compressive illumination scheme are comparable to that of random Toeplitz matrices with a much larger number of random elements. The proposed system is well matched to practical implementation utilizing a small number of random parameters and uniform sampling ADCs on receive. Our simulation show targets both on and off the grid can be detected using sparsity regularized recovery algorithms. A potential direction for future research is to investigate the effect of basis mismatch [90] due to targets not located on the grid locations and extend the theoretical guarantees to off the grid compressed sensing framework proposed in [14], [87] based on the generalization of notion of sparsity in an infinite dictionary setting [91]. We plan to investigate the effect of clutter by extending the analysis to a multi-pulse system and characterizing the ambiguity function.

REFERENCES

- M. A. Richards, Fundamentals of Radar Signal Processing. New York, NY, USA: McGraw-Hill, 2014.
- [2] N. Sugavanam and E. Ertin, "Interrupted SAR imaging with limited persistence scattering models," in *Proc. IEEE Radar Conf.*, 2017, pp. 1770–1775.
- [3] N. Sugavanam, E. Ertin, and R. Burkholder, "Compressing bistatic SAR target signatures with sparse-limited persistence scattering models," *IET Radar, Sonar Navigation*, vol. 13, no. 9, pp. 1411–1420, 2019.
- [4] N. Sugavanam and E. Ertin, "Limited persistence models for SAR automatic target recognition," in *Algorithms Synthetic Aperture Radar Imagery XXIV*, vol. 10201. International Society for Optics and Photonics, 2017, Art. no. 102010M.
- [5] P. Stoica and J. Li, MIMO Radar Signal Processing. Hoboken, NJ, USA: Wiley, 2008.
- [6] S. Baskar and E. Ertin, "A software defined radar platform for waveform adaptive MIMO radar research," in *Proc. IEEE Radar Conf.*, 2015, pp. 1590–1594.
- [7] R. H. Walden, "Analog-to-digital converter survey and analysis," *IEEE J. Sel. Areas Commun.*, vol. 17, no. 4, pp. 539–550, Apr. 1999.
- [8] R. Middleton, "Dechirp-on-receive linearly frequency modulated radar as a matched-filter detector," *IEEE Trans. Aerosp. Electron. Syst.*, vol. 48, no. 3, pp. 2716–2718, Jul. 2012.
- [9] Z. Ben-Haim, Y. C. Eldar, and M. Elad, "Coherence-based performance guarantees for estimating a sparse vector under random noise," *IEEE Trans. Signal Process.*, vol. 58, no. 10, pp. 5030–5043, Oct. 2010.
- [10] E. Candes, "The restricted isometry property and its implications for compressed sensing," *Comptes Rendus Mathematique*, vol. 346, no. 9–10, pp. 589–592, May 2008.
- [11] E. Candes and Y. Plan, "Near-ideal model selection by ℓ_1 minimization," *Ann. Statist.*, vol. 37, no. 5A, pp. 2145–2177, Oct. 2009.
- [12] E. Candes and T. Tao, "The Dantzig selector: Statistical estimation when P is much larger than N," Ann. Statist., vol. 35, no. 6, pp. 2313–2351, Dec. 2007.
- [13] R. Tibshirani, "Regression shrinkage and selection via the lasso," J. Roy. Stat. Soc.: Ser. B, vol. 73, no. 3, pp. 273–282, 1996.
- [14] G. Tang, B. N. Bhaskar, P. Shah, and B. Recht, "Compressed sensing off the grid," *IEEE Trans. Inf. Theory*, vol. 59, no. 11, pp. 7465–7490, Nov. 2013.
- [15] Z. Yang and L. Xie, "On gridless sparse methods for line spectral estimation from complete and incomplete data," *IEEE Trans. Signal Process.*, vol. 63, no. 12, pp. 3139–3153, Jun. 2015.
- [16] J. Tropp and A. Gilbert, "Signal recovery from random measurements via orthogonal matching pursuit," *IEEE Trans. Inf. Theory*, vol. 53, no. 12, pp. 4655–4666, Dec. 2007.
- [17] D. Needell and J. Tropp, "CoSaMP: Iterative signal recovery from incomplete and inaccurate samples," *Appl. Comput. Harmon. Anal.*, vol. 26, no. 3, pp. 301–321, 2009.
- [18] J. Liu, X. Chen, Z. Wang, and W. Yin, "ALISTA: Analytic weights are as good as learned weights in LISTA," in *Proc. Int. Conf. Learn. Representations*, 2019.
- [19] A. Aberdam, A. Golts, and M. Elad, "Ada-LISTA: Learned solvers adaptive to varying models," *IEEE Trans. Pattern Anal. Mach. Intell.*, to be published, doi: 10.1109/TPAMI.2021.3125041.
- [20] R. Fu, V. Monardo, T. Huang, and Y. Liu, "Theoretical linear convergence of deep unfolding network for block-sparse signal recovery," 2021, arXiv:2111.09801.
- [21] L. Potter, E. Ertin, J. Parker, and M. Cetin, "Sparsity and compressed sensing in radar imaging," *Proc. IEEE*, vol. 98, no. 6, pp. 1006–1020, Jun. 2010.
- [22] D. Cohen and Y. C. Eldar, "Sub-Nyquist radar systems: Temporal, spectral, and spatial compression," *IEEE Signal Process. Mag.*, vol. 35, no. 6, pp. 35–58, Nov. 2018.
- [23] R. Baraniuk and P. Steeghs, "Compressive radar imaging," in *Proc. IEEE Radar Conf.*, 2007, pp. 128–133.
- [24] K. Gedalyahu and Y. Eldar, "Time-delay estimation from low-rate samples: A union of subspaces approach," *IEEE Trans. Signal Process.*, vol. 58, no. 6, pp. 3017–3031, Jun. 2010.
- [25] M. Rossi, A. Haimovich, and Y. Eldar, "Spatial compressive sensing in MIMO radar with random arrays," in *Proc. 46th Ann. Conf. Inf. Sci. Syst.*, 2012, pp. 1–6.
- [26] D. Cohen, D. Cohen, Y. C. Eldar, and A. M. Haimovich, "SUMMeR: Sub-Nyquist MIMO radar," *IEEE Trans. Signal Process.*, vol. 66, no. 16, pp. 4315–4330, Aug. 2018.

- [27] O. Bar-Ilan and Y. C. Eldar, "Sub-Nyquist radar via Doppler focusing," IEEE Trans. Signal Process., vol. 62, no. 7, pp. 1796–1811, Apr. 2014.
- [28] S. Na, K. V. Mishra, Y. Liu, Y. C. Eldar, and X. Wang, "Tendsur: Tensor-based 4D sub-Nyquist radar," *IEEE Signal Process. Lett.*, vol. 26, no. 2, pp. 237–241, Feb. 2019.
- [29] D. Cohen, D. Cohen, and Y. C. Eldar, "High resolution FDMA MIMO radar," *IEEE Trans. Aerosp. Electron. Syst.*, vol. 56, no. 4, pp. 2806–2822, Aug. 2020.
- [30] E. Baransky, G. Itzhak, N. Wagner, I. Shmuel, E. Shoshan, and Y. Eldar, "Sub-Nyquist radar prototype: Hardware and algorithm," *IEEE Trans. Aerosp. Electron. Syst.*, vol. 50, no. 2, pp. 809–822, Apr. 2014.
- [31] K. V. Mishra, Y. C. Eldar, E. Shoshan, M. Namer, and M. Meltsin, "A cognitive sub-Nyquist MIMO radar prototype," *IEEE Trans. Aerosp. Electron. Syst.*, vol. 56, no. 2, pp. 937–955, Apr. 2020.
- [32] C.-Y. Chen and P. Vaidyanathan, "Compressed sensing in MIMO radar," in Proc. 42nd Asilomar Conf. Signals, Syst. Comput., 2008, pp. 41–44.
- [33] Y. Yu, A. Petropulu, and H. Poor, "CSSF MIMO radar: Compressive-sensing and step-frequency based MIMO radar," *IEEE Trans. Aerosp. Electron. Syst.*, vol. 48, no. 2, pp. 1490–1504, Apr. 2012.
- [34] B. Li and A. Petropulu, "RIP analysis of the measurement matrix for compressive sensing-based MIMO radars," in *Proc. IEEE 8th Sensor Array Multichannel Signal Process. Workshop*, 2014, pp. 497–500.
- [35] Y. Chi, "Sparse MIMO radar via structured matrix completion," in Proc. Glob. Conf. Signal Inf. Process., 2013, pp. 321–324.
- [36] S. Sun, W. Bajwa, and A. Petropulu, "MIMO-MC radar: A MIMO radar approach based on matrix completion," *IEEE Trans. Aerosp. Electron.* Syst., vol. 51, no. 3, pp. 1839–1852, Jul. 2015.
- [37] T. Huang, Y. Liu, H. Meng, and X. Wang, "Cognitive random stepped frequency radar with sparse recovery," *IEEE Trans. Aerosp. Electron. Syst.*, vol. 50, no. 2, pp. 858–870, Apr. 2014.
- [38] T. Huang, Y. Liu, X. Xu, Y. C. Eldar, and X. Wang, "Analysis of frequency agile radar via compressed sensing," *IEEE Trans. Signal Process.*, vol. 66, no. 23, pp. 6228–6240, Dec. 2018.
- [39] Y. Li, T. Huang, X. Xu, Y. Liu, L. Wang, and Y. C. Eldar, "Phase transitions in frequency agile radar using compressed sensing," *IEEE Trans. Signal Process.*, vol. 69, pp. 4801–4818, 2021, doi: 10.1109/TSP.2021.3099629.
- [40] T. Huang, N. Shlezinger, X. Xu, D. Ma, Y. Liu, and Y. C. Eldar, "Multi-carrier agile phased array radar," *IEEE Trans. Signal Process.*, vol. 68, pp. 5706–5721, 2020, doi: 10.1109/TSP.2020.3026186.
- [41] S. Sun and Y. D. Zhang, "4D automotive radar sensing for autonomous vehicles: A sparsity-oriented approach," *IEEE J. Sel. Topics Signal Process.*, vol. 15, no. 4, pp. 879–891, Jun. 2021.
- [42] K. V. Mishra, S. Mulleti, and Y. C. Eldar, "RaSSteR: Random sparse step-frequency radar," 2020, arXiv:2004.05720.
- [43] M. Herman and T. Strohmer, "High-resolution radar via compressed sensing," *IEEE Trans. Signal Process.*, vol. 57, no. 6, pp. 2275–2284, Jun. 2009.
- [44] T. Strohmer and B. Friedlander, "Analysis of sparse MIMO radar," Appl. Comput. Harmon. Anal., vol. 37, no. 3, pp. 361–388, 2014.
- [45] T. Strohmer and H. Wang, "Accurate imaging of moving targets via random sensor arrays and Kerdock codes," *Inverse Problems*, vol. 29, no. 8, 2013, Art. no. 085001.
- [46] D. Dorsch and H. Rauhut, "Refined analysis of sparse MIMO radar," J. Fourier Anal. Appl., vol. 23, no. 3, pp. 485–529, 2017.
- [47] M. Hugel, H. Rauhut, and T. Strohmer, "Remote sensing via \(\ell_1\)-minimization," Foundations Comput. Math., vol. 14, no. 1, pp. 115–150, 2014
- [48] M. Shastry, R. Narayanan, and M. Rangaswamy, "Sparsity-based signal processing for noise radar imaging," *IEEE Trans. Aerosp. Electron. Syst.*, vol. 51, no. 1, pp. 314–325, Jan. 2015.
- [49] J. Romberg, "Compressive sensing by random convolution," SIAM J. Img. Sci., vol. 2, no. 4, pp. 1098–1128, Nov. 2009.
- [50] R. Baraniuk, M. Davenport, R. A. DeVore, and M. B. Wakin, "A simple proof of the restricted isometry property for random matrices," *Construc*tive Approximation, vol. 28, no. 3, pp. 253–263, Dec. 2008.
- [51] J. Haupt, W. Bajwa, G. Raz, and R. Nowak, "Toeplitz compressed sensing matrices with applications to sparse channel estimation," *IEEE Trans. Inf. Theory*, vol. 56, no. 11, pp. 5862–5875, Nov. 2010.
- [52] H. Rauhut, J. Romberg, and J. A. Tropp, "Restricted isometries for partial random circulant matrices," *Appl. Comput. Harmon. Anal.*, vol. 32, no. 2, pp. 242–254, 2012.
- [53] F. Krahmer, S. Mendelson, and H. Rauhut, "Suprema of chaos processes and the restricted isometry property," *Commun. Pure Appl. Math.*, vol. 67, no. 11, pp. 1877–1904, 2014.

- [54] J. Tropp, J. Laska, M. Duarte, J. Romberg, and R. Baraniuk, "Beyond Nyquist: Efficient sampling of sparse bandlimited signals," *IEEE Trans. Inf. Theory*, vol. 56, no. 1, pp. 520–544, Jan. 2010.
- [55] J. Yoo *et al.*, "A compressed sensing parameter extraction platform for radar pulse signal acquisition," *IEEE Trans. Emerg. Sel. Topics Circuits Syst.*, vol. 2, no. 3, pp. 626–638, Sep. 2012.
- [56] M. A. Lexa, M. E. Davies, and J. S. Thompson, "Reconciling compressive sampling systems for spectrally sparse continuous-time signals," *IEEE Trans. Signal Process.*, vol. 60, no. 1, pp. 155–171, Jan. 2012.
- Trans. Signal Process., vol. 60, no. 1, pp. 155–171, Jan. 2012.
 [57] M. Mishali, Y. C. Eldar, and A. J. Elron, "Xampling: Signal acquisition and processing in union of subspaces," *IEEE Trans. Signal Process.*, vol. 59, no. 10, pp. 4719–4734, Oct. 2011.
- [58] T. T. Cai and T. Jiang, "Limiting laws of coherence of random matrices with applications to testing covariance structure and construction of compressed sensing matrices," Ann. Statist., vol. 39, no. 3, pp. 1496–1525, Jun. 2011.
- [59] K. Davidson and S. Szarek, "Local operator theory, random matrices and banach spaces," *Handbook Geometry Banach Spaces*, vol. 1, pp. 317–366, 2001.
- [60] W. Bajwa, "Geometry of random Toeplitz-block sensing matrices: Bounds and implications for sparse signal processing," *Proc. SPIE*, vol. 8365, pp. 836505–836505-7, 2012.
- [61] K. V. Mishra, Y. C. Eldar, A. Maio, and A. Haimovich, "Sub-Nyquist radar: Principles and prototypes," in *Compressed Sensing in Radar Signal Processing*. Cambridge, U.K.: Cambridge Univ. Press, 2019, pp. 1–48.
- [62] E. Ertin, "Frequency diverse waveforms for compressive radar sensing," in *Proc. Int. Waveform Diversity Des. Conf.*, 2010, pp. 000216–000219.
- [63] N. Sugavanam and E. Ertin, "Recovery guarantees for multifrequency chirp waveforms in compressed radar sensing," 2015, arXiv:1508.07969.
- [64] E. Ertin, L. Potter, and R. Moses, "Sparse target recovery performance of multi-frequency chirp waveforms," in *Proc. 19th Eur. Signal Process. Conf.*, 2011, pp. 446–450.
- [65] N. Sugavanam, S. Baskar, and E. Ertin, "Recovery guarantees for high resolution radar sensing with compressive illumination," in *Proc. 4th Int.* Workshop Compressed Sens. Theory Appl. Radar, Sonar Remote Sens., 2016, pp. 252–256.
- [66] N. Sugavanam, "Compressive sampling in radar imaging," Ph.D. dissertation, The Ohio State Univ., 2017.
- [67] P. Brennan, Y. Huang, M. Ash, and K. Chetty, "Determination of sweep linearity requirements in FMCW radar systems based on simple voltagecontrolled oscillator sources," *IEEE Trans. Aerosp. Electron. Syst.*, vol. 47, no. 3, pp. 1594–1604, Jul. 2011.
- [68] J.-W. Ting, D. Oloumi, and K. Rambabu, "FMCW SAR system for near-distance imaging applications-practical considerations and calibrations," *IEEE Trans. Microw. Theory Techn.*, vol. 66, no. 1, pp. 450–461, Jan. 2018.
- [69] S. Ayhan, S. Scherr, A. Bhutani, B. Fischbach, M. Pauli, and T. Zwick, "Impact of frequency ramp nonlinearity, phase noise, and SNR on FMCW radar accuracy," *IEEE Trans. Microw. Theory Techn.*, vol. 64, no. 10, pp. 3290–3301, Oct. 2016.
- [70] B. Rigling, W. Garber, R. Hawley, and L. Gorham, "Wide-area, persistent SAR imaging: Algorithm tradeoffs," *IEEE Aerosp. Electron. Syst. Mag.*, vol. 29, no. 1, pp. 14–20, Jan. 2014.
- [71] N. Sugavanam and E. Ertin, "Recovery guarantees for MIMO radar using multi-frequency LFM waveform," in *Proc. IEEE Radar Conf.*, 2016, pp. 1–6.

- [72] G. San Antonio, D. R. Fuhrmann, and F. C. Robey, "MIMO radar ambiguity functions," *IEEE J. Sel. Topics Signal Process.*, vol. 1, no. 1, pp. 167–177, Jun. 2007.
- [73] X. Long, K. Li, J. Tian, J. Wang, and S. Wu, "Ambiguity function analysis of random frequency and PRI agile signals," *IEEE Trans. Aerosp. Electron.* Syst., vol. 57, no. 1, pp. 382–396, Feb. 2021.
- [74] D. L. Donoho, "Compressed sensing," *IEEE Trans. Inf. Theory*, vol. 52, no. 4, pp. 1289–1306, Apr. 2006.
- [75] S. Foucart and H. Rauhut, *A Mathematical Introduction to Compressive Sensing*. Basel, Switzerland: Birkhauser, 2013.
- [76] S. S. Chen, D. L. Donoho, and M. A. Saunders, "Atomic decomposition by basis pursuit," SIAM Rev., vol. 43, no. 1, pp. 129–159, Jan. 2001.
- [77] M. Talagrand, Upper and Lower Bounds for Stochastic Processes. Berlin, Germany: Springer, 2014.
- [78] N. Boyd, G. Schiebinger, and B. Recht, "The alternating descent conditional gradient method for sparse inverse problems," *SIAM J. Optim.*, vol. 27, no. 2, pp. 616–639, 2017. [Online]. Available: http://dx.doi.org/10.1137/15M1035793
- 79] Y. Yu, X. Zhang, and D. Schuurmans, "Generalized conditional gradient for sparse estimation," *J. Mach. Learn. Res.*, vol. 18, no. 144, pp. 1–46, 2017.
- [80] A. Beck and M. Teboulle, "A fast iterative shrinkage-thresholding algorithm for linear inverse problems," SIAM J. Imag. Sci., vol. 2, no. 1, pp. 183–202, 2009.
- [81] L. Chizat, "Sparse optimization on measures with over-parameterized gradient descent," *Math. Program.*, pp. 1–46, Mar. 2021, doi: 10.1007/s10107-021-01636-z.
- [82] W. Li, W. Liao, and A. Fannjiang, "Super-resolution limit of the ESPRIT algorithm," *IEEE Trans. Inf. Theory*, vol. 66, no. 7, pp. 4593–4608, Jul. 2020.
- [83] A. Fannjiang and W. Liao, "Coherence pattern-guided compressive sensing with unresolved grids," SIAM J. Imag. Sci., vol. 5, no. 1, pp. 179–202, 2012
- [84] K. Mahata and M. M. Hyder, "Fast frequency estimation with prior information," *IEEE Trans. Signal Process.*, vol. 66, no. 1, pp. 264–273, Jan. 2018.
- [85] K. V. Mishra, M. Cho, A. Kruger, and W. Xu, "Spectral super-resolution with prior knowledge," *IEEE Trans. Signal Process.*, vol. 63, no. 20, pp. 5342–5357, Oct. 2015.
- [86] M. Cho, K. V. Mishra, J.-F. Cai, and W. Xu, "Block iterative reweighted algorithms for super-resolution of spectrally sparse signals," *IEEE Signal Process. Lett.*, vol. 22, no. 12, pp. 2319–2313, Dec. 2015.
- [87] G. Tang, B. Bhaskar, and B. Recht, "Near minimax line spectral estimation," *IEEE Trans. Inf. Theory*, vol. 61, no. 1, pp. 499–512, Jan. 2015.
- [88] N. Sugavanam, S. Baskar, and E. Ertin, "High resolution radar sensing with compressive illumination," 2021, arXiv:2106.11490.
- [89] M. Rudelson and R. Vershynin, "Hanson-Wright inequality and sub-gaussian concentration," *Electron. Commun. Probab.*, vol. 18, pp. 1–9, 2013
- [90] Y. Chi, L. Scharf, A. Pezeshki, and A. Calderbank, "Sensitivity to basis mismatch in compressed sensing," *IEEE Trans. Signal Process.*, vol. 59, no. 5, pp. 2182–2195, May 2011.
- [91] V. Chandrasekaran, B. Recht, P. A. Parrilo, and A. S. Willsky, "The convex geometry of linear inverse problems," *Foundations Comput. Math.*, vol. 12, no. 6, pp. 805–849, 2012.